Sequential changes in ocean circulation and biological export productivity during the last glacial cycle: a model-data study

Cameron M. O'Neill[1], Andrew McC. Hogg[1,2], Michael J. Ellwood[1], Bradley N. Opdyke[1], and Stephen M. Eggins[1]

[1]Research School of Earth Sciences, Australian National University, Canberra, Australia
[2]ARC Centre of Excellence for Climate Extremes, Australian National University, Canberra, Australia

Correspondence to: Cameron O'Neill (cameron.oneill@anu.edu.au)

Abstract.

We conduct a model-data analysis of the marine carbon cycle to understand and quantify the drivers of atmospheric CO_2 during the last glacial cycle. We use a carbon cycle box model "SCP-M", combined with multiple proxy data for the atmosphere and ocean, to test for variations in ocean circulation and Southern Ocean biological export productivity across marine isotope stages spanning 130 thousand years ago to the present. The model is constrained by proxy data associated with a range of environmental conditions including sea surface temperature, salinity, ocean volume, sea-ice cover and shallow water carbonate production. Model parameters for global ocean circulation, Atlantic meridional overturning circulation and Southern Ocean biological export productivity are optimised in each marine isotope stage, against proxy data for atmospheric CO_2, $\delta^{13}C$ and $\Delta^{14}C$ and deep ocean $\delta^{13}C$, $\Delta^{14}C$ and carbonate ion. Our model-data results suggest that global overturning circulation weakened at marine isotope stage 5d, coincident with a $\sim$25 ppm fall in atmospheric CO_2 from the penultimate interglacial level. This change was followed by a further slowdown in Atlantic meridional overturning circulation and enhanced Southern Ocean biological export productivity at marine isotope stage 4 ($\sim$-30 ppm). There was also a transient slowdown in Atlantic meridional overturning circulation at MIS 5b. In this model, the last glacial maximum was characterised by relatively weak global ocean and Atlantic meridional overturning circulation, and increased Southern Ocean biological export productivity ($\sim$-20 ppm during MIS 2-4). Ocean circulation and Southern Ocean biology rebounded to modern values by the Holocene period. The terrestrial biosphere decreased by $\sim$400 Pg C in the lead up to the last glacial maximum, followed by a period of intense regrowth during the Holocene ($\sim$630 Pg C). Slowing ocean circulation, a cooler ocean and, to a lesser extent, shallow carbonate dissolution, contributed $\sim$-75 ppm to atmospheric CO_2 in the $\sim$100 thousand-year lead-up to the last glacial maximum, with a further $\sim$-10 ppm contributed during the glacial maximum. Our model results also suggest that an increase in Southern Ocean biological productivity was one of the ingredients required to achieve the last glacial maximum atmospheric CO_2 level. The incorporation of longer-timescale data into quantitative ocean transport models, provides useful insights into the timing of changes in ocean processes, enhancing our understanding of the last glacial maximum and Holocene carbon cycle transition.

1 Introduction

Large and regular fluctuations in atmospheric CO_2 and ocean proxy signals for carbon isotopes and carbonate ion concentration, over the last 800 kyr, are preserved in ice and marine core records. The most obvious of these fluctuations is the repeated oscillation of atmospheric CO_2 over the range of $\sim$180-280 ppm every $\sim$100 kyr. The magnitude and regularity of these oscillations in atmospheric CO_2, combined with proxy observations for carbon isotopes, point to the quasi-regular transfer of carbon between the main earth reservoirs: the ocean, atmosphere, terrestrial biosphere and marine sediments (Broecker, 1982; Sigman and Boyle, 2000; Toggweiler, 2008; Hogg, 2008; Kohfeld and Ridgewell, 2009; Kohfeld and Chase, 2017). The ocean, given its large size as a carbon store and ongoing exchange of CO_2 with the atmosphere, likely plays the key role in changing atmospheric CO_2 (Broecker, 1982; Knox and McElroy, 1984; Toggweiler and Sarmiento, 1985; Sigman and Boyle, 2000; Kohfeld and Ridgewell, 2009). Ocean-centric hypotheses for variation in atmospheric CO_2 have been examined in great detail for the last glacial maximum (LGM) and Holocene periods, supported by the abundance of paleo data from marine sediment coring and sampling activity (e.g. Sikes et al., 2000; Curry and Oppo, 2005; Kohfeld and Ridgewell, 2009; Oliver et al., 2010; Menviel et al., 2012; Peterson et al., 2014; Yu et al., 2014b; Menviel et al., 2016; Skinner et al., 2017; Muglia et al., 2018; Yu et al., 2019). However, the hypotheses for variation in atmospheric CO_2 across the LGM-Holocene remain under debate (e.g. Kohfeld et al., 2005; Martinez-Garcia et al., 2014; Menviel et al., 2016; Skinner et al., 2017; Muglia et al., 2018; Khatiwala et al., 2019). Established hypotheses include those emphasising ocean biology (e.g. Martin, 1990; Martinez-Garcia et al., 2014), ocean circulation (e.g. Burke and Robinson, 2012; Menviel et al., 2016; Skinner et al., 2017), or the aggregate effect of several mechanisms (e.g. Kohfeld and Ridgewell, 2009; Hain et al., 2010; Ferrari et al., 2014; Ganopolski and Brovkin, 2017; Muglia et al., 2018) to explain the LGM-Holocene carbon cycle transition. Hypotheses for an ocean biological role include the effects of iron fertilisation on biological export productivity (e.g. Martin, 1990; Watson et al., 2000; Martinez-Garcia et al., 2014), the depth of remineralisation of particulate organic carbon (POC) (e.g. Matsumoto, 2007; Kwon et al., 2009; Menviel et al., 2012), changes in the organic carbon:carbonate ("the rain ratio") or carbon:silicate constitution of marine organisms (e.g. Archer and Maier-Reimer, 1994; Harrison, 2000), and increased biological utilisation of exposed shelf-derived nutrients such as phosphorus (e.g. Menviel et al., 2012).

Several studies have attempted to solve the problem of glacial-interglacial CO_2 by modelling either the last glacial-interglacial cycle in its entirety, or multiple glacial-interglacial cycles (e.g. Ganopolski et al., 2010; Menviel et al., 2012; Brovkin et al., 2012; Ganopolski and Brovkin, 2017). These studies highlight the roles of orbitally-forced Northern Hemisphere ice sheets in the onset of the glacial periods, and important feedbacks from ocean circulation, carbonate chemistry and marine biological productivity throughout the glacial cycle (Ganopolski et al., 2010; Brovkin et al., 2012; Ganopolski and Brovkin, 2017). Menviel et al. (2012) modelled a range of physical and biogechemical mechanisms to deliver the full amplitude of atmospheric CO_2 variation in the last glacial-interglacial cycle, using transient simulations with the Bern3D model. According to Brovkin et al. (2012), a $\sim$50 ppm drop in atmospheric CO_2 early in the last glacial cycle was caused by cooling sea surface temperatures (SST), increased Northern hemisphere ice sheet cover, and expansion of southern-sourced abyssal waters in place of North Atlantic Deep Water (NADW) formation. Ganopolski and Brovkin (2017) modelled the last four glacial cycles with orbital forcing as the singular driver of carbon cycle feedbacks. They described the "carbon stew", a feedback of combined physical and biogeochemical changes in the carbon cycle, to drive the last four glacial-interglacial cycles of atmospheric CO_2.

Kohfeld and Chase (2017) also extended the LGM-Holocene CO_2 debate further into the past, by evaluating proxy data over the period 18-115 thousand years before present (ka), a time that encompasses the gradual fall in atmospheric CO_2 of ~85-90 ppm from the penultimate interglacial period until the last glacial termination. Kohfeld and Chase (2017) identified time periods during which CO_2 decreased, and aligned these with concomitant changes in proxies for SST, sea-ice extent, deep Atlantic Ocean circulation and mixing, and ocean biological productivity. Kohfeld and Chase (2017) observed that the ~100kyr transition to the LGM involved three discrete CO_2 events. Firstly, a drop in atmospheric CO_2 of ~35 ppm at ~115-100 ka (marine isotope stage, or MIS, 5c-5d) was accompanied by lower SST and the expansion of Antarctic sea-ice cover. A second phase of CO_2 drawdown took place ~72-65 ka (MIS 4-5a), of ~40ppm, and likely resulted from a slowdown in deep ocean circulation (Kohfeld and Chase, 2017). Finally, during the period 40-18 ka (MIS 2-4), atmospheric CO_2 dropped a further 5-10 ppm, which according to Kohfeld and Chase (2017), was the result of enhanced Southern Ocean biological productivity, and continually intensifying deep ocean stratification, including shoaling of North Atlantic Deep Water (NADW) and northward extension of Antarctic Bottom Water (AABW).

In this paper we quantitatively test the Kohfeld and Chase (2017) hypothesis by undertaking model-data experiments in each MIS across the last glacial cycle, and extend their analysis to include Pacific and Indian Ocean modelling and proxy data. We use the SST reconstructions compiled by Kohfeld and Chase (2017) and other glacial cycle proxies presented in that work. We apply a carbon cycle box model (O'Neill et al., 2019), constrained by available atmospheric and oceanic proxy data, to solve for optimal model-data parameter solutions for ocean circulation and biological export productivity. We also present a qualitative analysis of the compiled proxy data, to place the model-data experiment results in context. We thereby further constrain the timing and magnitude of posited CO_2 mechanisms operating during each MIS in the last glacial cycle (e.g. Kohfeld and Ridgewell, 2009; Oliver et al., 2010; Menviel et al., 2012; Brovkin et al., 2012; Yu et al., 2013; Eggleston et al., 2016; Yu et al., 2016; Kohfeld and Chase, 2017). This time series analysis complements recent multi-proxy model-data studies of the LGM and Holocene (e.g. Menviel et al., 2016; Kurahashi-Nakamura et al., 2017; Muglia et al., 2018; O'Neill et al., 2019) by testing for changes in the ocean carbon cycle in the lead-up to the LGM, in addition to the LGM-to-Holocene. Our modelling approach differs from other model studies of the last glacial-interglacial cycle (e.g. Ganopolski et al., 2010; Menviel et al., 2012; Brovkin et al., 2012; Ganopolski and Brovkin, 2017), in that we constrain several physical processes from observations (SST, sea level, sea-ice cover, salinity, coral reef fluxes of carbon), then solve for the values of model parameters for ocean circulation and biology based on an optimisation against atmospheric and ocean proxy data.

2 Materials and methods

2.1 Model description

We used the SCP-M carbon cycle box model in our model-data experiment (O'Neill et al., 2019). In summary, SCP-M contains simple parameterisations of the major fluxes in the Earth's surface carbon cycle (Fig. 1). SCP-M incorporates the ocean,

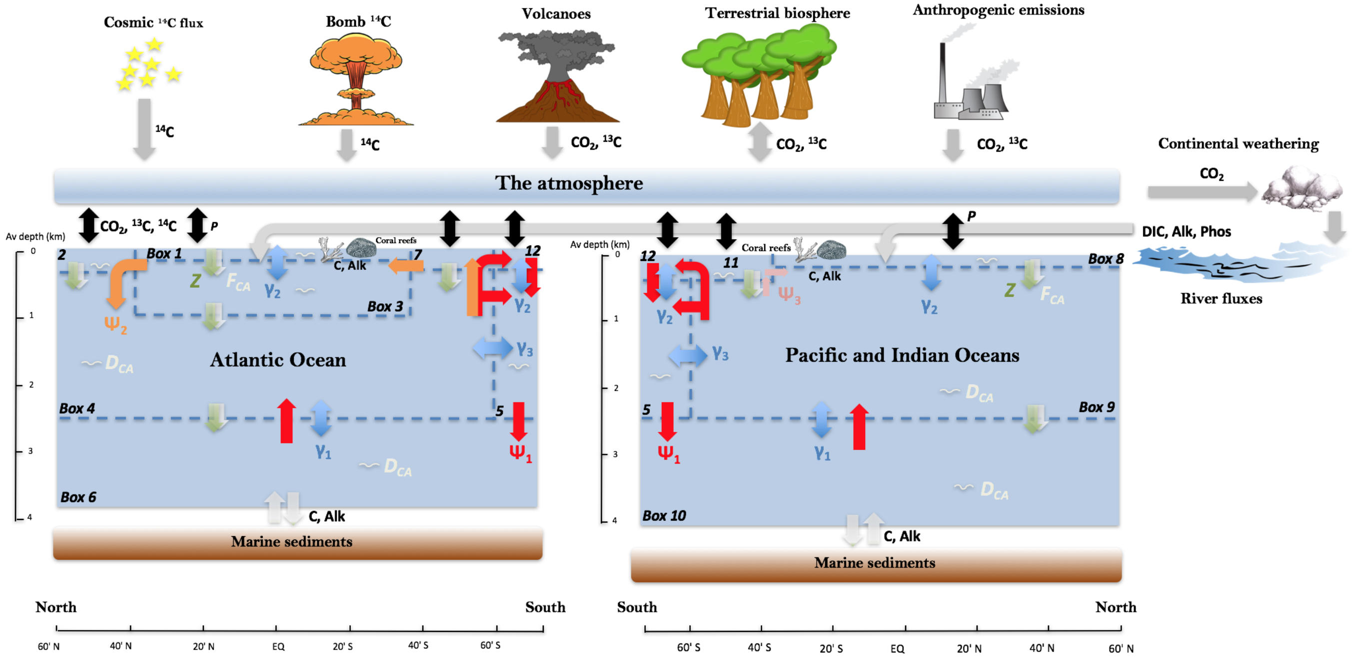

Figure 1. SCP-M configured as a twelve box ocean model-plus atmosphere with marine sediments, continents and the terrestrial biosphere. Exchange of elemental concentrations occur due to fluxes between boxes. Ψ_1 (red arrows) is global overturning circulation (GOC), Ψ_2 (orange arrows) is Atlantic meridional overturning circulation (AMOC). GOC upwelling in both basins is set by default to 50% split between upwelling into the subpolar and polar Southern Ocean. Ψ_3 (pink arrows) is Antarctic intermediate water (AAIW) and Subantarctic mode water (SAMW) formation in the Indian and Pacific Oceans (e.g. Talley, 2013). Blue arrows represent mixing fluxes between boxes. γ_1 and γ_3 parameterise deep-abyssal and Southern Ocean-deep topographically-induced mixing (e.g. De Boer and Hogg, 2014), while γ_2 is low-latitude thermohaline mixing (e.g. Liu et al., 2016). Z (green downward arrows) is the biological pump, F_{CA} (white downward arrows) is the carbonate pump, D_{CA} (white squiggles) is carbonate dissolution and P (black, bidirectional arrows) is the air-sea gas exchange. Key to boxes: Atlantic (box 1: low latitude/tropical surface ocean, 0-100m; box 2: northern surface ocean, 0-250m; box 3: intermediate ocean, 100-1,000m; box 4: deep ocean, 1,000-2,500m; box 6: abyssal ocean, 2,500-3,700m; box 7: subpolar southern surface ocean, 0-250m). Pacific-Indian (box 8: low latitude/tropical surface ocean, 0-100m; box 9: deep ocean, 100-2,500m; box 10: abyssal ocean, 2,500-4,000m; box 11: subpolar southern surface ocean, 0-250m). Southern Ocean (box 5: intermediate-deep; box 12: surface ocean). For a more detailed model description see O'Neill et al. (2019) and updated model code and data at https://doi.org/10.5281/zenodo.3559339.

atmosphere, terrestrial biosphere and marine/continental sediment carbon reservoirs, weathering and river fluxes, and a number of variables including atmospheric CO_2, DIC, phosphorus, alkalinity, carbon isotopes (^{13}C and ^{14}C) and the carbonate ion. SCP-M calculates ocean pCO_2 using the equations of Follows et al. (2006), and applies the first and second "dissociation constants" of carbonic acid estimated by Lueker et al. (2000), to calculate HCO_3^- and CO_3^{2-} concentrations, respectively, in units of μmol kg^{-1}, in each ocean box. The model employs partial differential equations for determining the concentration of elements in each box, with each box represented as a row and column in a matrix. In this paper, we extend SCP-M by incorporating a separate basin for the combined Pacific and Indian Oceans (Fig. 1), following the conceptual model of Talley (2013), to incorporate modelling and proxy data for those regions of the ocean. This version of SCP-M consists of 12 ocean boxes plus the atmosphere and terrestrial biosphere. SCP-M splits out depth regions of the ocean between surface boxes (100-250m average depth), intermediate (1,000m average depth), deep (2,500m average depth) and abyssal depth boxes (3,700 (Atlantic) - 4,000m (Pacific-Indian) average depth). The Southern Ocean is split into two boxes, including a polar box which covers latitude range 60-80 degrees South (box 12 in Fig. 1) and subpolar boxes in the Atlantic (box 7) and Pacific-Indian (box 12) basins, which cover latitude range 40-60 degrees South. See O'Neill et al. (2019) for a discussion of the choice of box depth and latitude dimensions.

The major ocean carbon flux parameters of interest in this model-data study, are global ocean circulation (GOC), Ψ_1, Atlantic meridional overturning circulation (AMOC), Ψ_2, and ocean biological export productivity, Z. The ocean circulation parameters Ψ_1 and Ψ_2 are simply prescribed in units of Sverdrups (Sv, 10^6 m^3 s^{-1}). Ocean biological export productivity Z is calculated using the method of Martin et al. (1987). The biological productivity flux, at 100m depth, is attenuated with depth for each box according to the decay rule of Martin et al. (1987). Each sub surface box receives a biological flux of an element at its ceiling depth, and loses a flux at its floor depth (lost to the boxes below it). The difference is the amount of element that is remineralised into each box. The input parameter is the value of export production at 100m depth, in units of mol C m^{-2} yr^{-1} as per Martin et al. (1987). Equation (1) shows the general form of the Martin et al. (1987) equation:

$$F = F_{100}(\frac{d}{100})^b \tag{1}$$

Where F is a flux of carbon in mol C m^{-2} yr^{-1}, F_{100} is an estimate of carbon flux at 100m depth, d is depth in metres and b is a depth scalar. In SCP-M, the Z parameter implements the Martin et al. (1987) equation. Z is an estimate of biological productivity at 100m depth (in mol C m^{-2} yr^{-1}), and coupled with the Martin et al. (1987) depth scalar, controls the amount of organic carbon that sinks from each model surface box to the boxes below.

The terrestrial biosphere is represented in SCP-M as a stock of carbon (a box) that fluxes with the atmosphere, governed by parameters for net primary productivity (NPP) and respiration. In SCP-M, NPP is calculated as a function of carbon fertilisation, which increases NPP as atmospheric CO$_2$ rises via a simple logarithmic relationship, using the model of Harman et al. (2011). This is a simplified approach, which omits the contribution of temperature and precipitation on NPP. Other, more complex models of the carbon cycle applied to glacial-interglacial cycles have a more detailed treatment of the terrestrial biosphere, including climate dependencies (e.g. Brovkin et al., 2002; Menviel et al., 2012). A number of studies emphasise the role of atmospheric CO$_2$ as the driver of terrestrial biosphere NPP on glacial-interglacial cycles (Kaplan et al., 2002; Otto et al., 2002; Joos et al., 2004; Hoogakker et al., 2016), although other studies cast doubt on the relative importance of atmospheric CO$_2$ versus temperature and precipitation (Francois et al., 1999; van der Sleen et al., 2015).

The isotopic fractionation behaviour of the terrestrial biosphere may also vary on glacial-interglacial timeframes. This has been studied for the LGM, Holocene and the present day (e.g. Collatz et al., 1998; Francois et al., 1999; Kaplan et al., 2002; Kohler and Fischer, 2004; Joos et al., 2004; Kohn, 2016). The variation in isotopic fractionation within the terrestrial biosphere reflects changes in the relative proportions of plants with the C3 and C4 photosynthetic pathways, but also strong variations within the same photosynthetic pathways themselves (Francois et al., 1999; Kohn, 2010; Schubert and Jahren, 2012; Kohn, 2016). The drivers for these changes include relative sea level and exposed land surface area (Francois et al., 1999), global tree-line extent (Kohler and Fischer, 2004), atmospheric temperature and CO_2 (Collatz et al., 1998; Francois et al., 1999; Kohler and Fischer, 2004; Kohn, 2010; Schubert and Jahren, 2012), global and localised precipitation and humidity (Huang et al., 2001; Kohn, 2010; Schubert and Jahren, 2012; Kohn, 2016), and also changes in the intercellular CO_2 pressure in the leaves of C3 plants (Francois et al., 1999). Estimated changes in average terrestrial biosphere δ^{13}C signature between the LGM and the Holocene fall in the range -0.3-1.8‰ (less negative δ^{13}C signature in the LGM), with further changes estimated from the onset of the Holocene to the pre-industrial, and even greater changes to the present day (due to rising atmospheric CO_2). This feature has been covered in detail within studies that focussed on the terrestrial biosphere between the LGM and Holocene, but less so in modelling and model-data studies of the last glacial-interglacial cycle. Menviel et al. (2016) provided a sensitivity of -0.7+0.5‰ around an average LGM terrestrial biosphere value δ^{13}C of -23.3‰, based on previous modelling of the LGM-Holocene timeframe by Joos et al. (2004). Another modelling study (Menviel and Joos, 2012), assessed the variation in LGM-Holocene δ^{13}C of the terrestrial biosphere to be a minor factor and it was omitted. Kohler and Fischer (2004) assessed the changing δ^{13}C signature of plants between the LGM and Holocene to be a minor factor in setting δ^{13}C of marine DIC, compared to changes in the absolute size of the terrestrial biosphere across this period. Given the uncertainty and ranges of starting estimates of terrestrial biosphere δ^{13}C, the uncertain LGM-Holocene changes, the large number of potential drivers, and the further uncertainty in extrapolating the posited LGM-Holocene changes back for the preceding 100 kyr, and the modest changes relative to the average δ^{13}C signature (and the very large range in, for example, present day estimates of C3 plant δ^{13}C (Kohn, 2010, 2016), we omit this feature with the caveat that there is added uncertainty in our terrestrial biosphere results with respect of the δ^{13}C signature applied. We apply an average δ^{13}C signature of -23‰, similar to values assumed by Menviel et al. (2016) and Jeltsch-Thommes et al. (2019) (23.3‰, -24‰ respectively), but more negative than assumed in Brovkin et al. (2002), Kohler and Fischer (2004) and Joos et al. (2004) (-16-(-17)‰). Our aim is not to contribute new findings of the terrestrial biosphere, but to ensure that the simple representation of the terrestrial biosphere in SCP-M provides the appropriate feedbacks to our (exhaustive) glacial-interglacial cycle model-data optimisation experiments, that are in line with published estimates.

Air-sea gas exchange is based on the relative pCO_2 in the surface ocean boxes and the atmosphere, and a parameter that sets its rate in m day^{-1}, P (Fig. 1), with ocean pCO_2 calculated using the method of Follows et al. (2006). SCP-M parameterises shallow water carbonate production, which is linked to the Z parameter by an assumption for the relative proportion of carbonate vs organic matter, known as "the rain ratio" (e.g. Archer and Maier-Reimer, 1994; Ridgwell, 2003). Carbonate dissolution is calculated based on the ocean box or marine surface sediment calcium carbonate concentration versus a depth-dependant saturation concentration (Morse and Berner, 1972; Millero, 1983). Most other carbon cycle processes are parameterised simply, such as volcanic emissions, continental weathering, anthropogenic emissions and cosmic ^{14}C fluxes. The isotopes of carbon are calculated applying various fractionation factors associated with the biological, physical and chemical fluxes of carbon (see the Supporting Information and O'Neill et al. (2019)).

We have added a simple representation of shallow water carbonate fluxes of carbon and alkalinity in SCP-M's low latitude surface boxes, to cater for this feature in theories for glacial cycle CO_2 (e.g. Berger, 1982; Opdyke and Walker, 1992; Ridgwell et al., 2003; Vecsei and Berger, 2004; Menviel and Joos, 2012), using:

$$\left[\frac{dC_i}{dt}\right]_{reef} = C_{reef}/V_i \tag{2}$$

Where C_{reef} is the prescribed flux of carbon out of/into the low latitude surface ocean boxes during net reef accumulation/dissolution, in mol C yr^{-1}, and V_i is the volume of the low latitude surface box i. The alkalinity flux associated with reef production/dissolution is simply Eq. 2 multiplied by two (e.g. Sarmiento and Gruber, 2006).

The major fluxes of carbon are parameterised simply in SCP-M to allow them to be solved by model-data optimisation with respect of atmospheric and ocean proxy data. In this study, the values for GOC, AMOC and biological export productivity at 100m depth, are outputs of the model-data experiments, as they are deduced from a data optimisation routine. Their input values for the experiments are ranges, as described in 2.2.1. SCP-M's fast run time and flexibility renders it useful for long term paleo-reconstructions involving large numbers of quantitative experiments and data integration (O'Neill et al., 2019). SCP-M is a simple box model, which incorporates large regions of the ocean as averaged boxes and parameterised fluxes. It is an appropriate tool for this study, in which we evaluate many tens of thousands of simulations to explore possible parameter combinations, in conjunction with proxy data. The model used for this paper is located at https://doi.org/10.5281/zenodo.3559339.

2.2 Model-data experiment design

We undertook a series of model-data experiments to solve for the values of ocean circulation and biology parameters at each MIS stage during the last glacial cycle (0-130 ka). We targeted these parameters due to their central role in many LGM-Holocene CO_2 hypotheses (e.g. Knox and McElroy, 1984; Toggweiler and Sarmiento, 1985; Martin, 1990; Kohfeld and Ridgewell, 2009; Hain et al., 2010; Sigman et al., 2010; Yu et al., 2014a; Menviel et al., 2016; Kohfeld and Chase, 2017; Muglia et al., 2018). We force SST, salinity, sea volume and ice cover, and reef carbonate production, in each MIS (Section 2.2.1, Fig. 2), using values sourced from the literature (e.g. Opdyke and Walker, 1992; Key, 2001; Adkins et al., 2002; Ridgwell et al., 2003; Kohfeld and Ridgewell, 2009; Rohling et al., 2009; Wolff et al., 2010; Muscheler et al., 2014; Kohfeld and Chase, 2017). Then, we optimise the model parameters for GOC, AMOC and Southern Ocean biological export productivity in each MIS time slice. We chose GOC and AMOC due to the prevalence of varying ocean circulation in many theories for glacial cycles of CO_2 (e.g. Sarmiento and Toggweiler, 1984; Toggweiler, 1999; Kohfeld and Ridgewell, 2009; Burke and Robinson, 2012; Freeman et al., 2016; Menviel et al., 2016; Kohfeld and Chase, 2017; Skinner et al., 2017; Muglia et al., 2018), and its key role in distribution of carbon and other elements in the ocean (Talley, 2013). We chose to vary Southern Ocean biological export productivity due to its long-standing place and debate among theories of atmospheric CO_2 during the LGM and Holocene (e.g. Martin, 1990; Knox and McElroy, 1984; Sarmiento and Toggweiler, 1984; Sigman and Boyle, 2000; Anderson et al., 2002; Kohfeld and Ridgewell, 2009; Martinez-Garcia et al., 2014; Menviel et al., 2016; Kohfeld and Chase, 2017; Muglia et al., 2018).

The GOC (Ψ_1), AMOC (Ψ_2) and Southern Ocean biology (Z) parameters are varied over ~9,000 possible combinations at each MIS, a total of ~80,000 simulations across MIS 1-5e. At the end of each experiment batch, the model results are solved for the best fit to the ocean and atmosphere proxy data using a least-squares optimisation, and the parameter values for Ψ_1, Ψ_2 and Z are returned. Our experiment time slices are the MIS of Lisiecki and Raymo (2005), with two minor modifications (see Fig. 2). MIS 2 (14-29 ka) as per Lisiecki and Raymo (2005) straddles the LGM (18-24 ka) and the last glacial termination (15-18 ka), while MIS 1 (0-14 ka) incorporates the Holocene period (0-11.7 ka) and the end of the termination. We are interested in the LGM and Holocene as discrete periods, so our experiment time slice for MIS 2 is truncated at 18 ka, and our MIS 1 simply covers the Holocene, removing overlaps with the glacial termination. Therefore, our modelling excludes the last glacial termination (~11-18 ka). The glacial termination period was highly transient, with atmospheric CO_2 varying by ~85 ppm in $<$10 kyr, and large changes in carbon isotopes. Thus it is anticipated that in a model-data reconstruction, model parameters would vary substantially for this period. Our strategy of integrating the model forward to an equilibrium state for each MIS as intervals of discrete climate and CO_2, would be unsuitable when applied to the last glacial termination. Joos et al. (2004), Ganopolski et al. (2010), Menviel et al. (2012), Menviel and Joos (2012), Brovkin et al. (2012) and Ganopolski and Brovkin (2017) provide coverage of the termination period with transient simulations of the last glacial-interglacial cycle, using intermediate complexity models (more complex than our model). For MIS 5, we take the timing for peak glacial and interglacial substages of Lisiecki and Raymo (2005), ±5kyr for MIS 5c-5e, and ±2.5 kyr for MIS 5a-5b.

2.2.1 Model forcings and parameter variations

We took a reconstructed SST time series for the last 130 kyr (Kohfeld and Chase, 2017), mapped these to SCP-M's surface boxes, and averaged the time series across each MIS (Fig. 2(A)). We have extrapolated an Antarctic sea ice cover proxy as shown in Fig. 2(B) (Wolff et al., 2010) to the profiles for sea surface salinity (Fig. 2(C)) and the polar Southern Ocean box air-sea gas exchange parameter (Fig. 2(D). For example, our notional reduction in the strength of the polar Southern Ocean box air-sea gas exchange due to Antarctic sea ice cover (-30%) is linearly (negatively) profiled with the Antarctic sea ice proxy time series of Wolff et al. (2010). We also vary the North Atlantic air-sea gas exchange parameter to the same extent (-30%) to approximate the effects of increased sea ice during MIS 2 and MIS 4 (Hoff et al., 2015; Maffezzoli et al., 2018). Note the polar Southern Ocean box, which is forced with reduced air-sea exchange, is separate from the subpolar Southern Box in which the biological export productivity parameter is varied in the model-data experiment. Our treatment of sea-ice cover is simply as a regulator of air-sea gas exchange in the polar ocean surface boxes. This treatment misses important linkages that likely exist between sea-ice cover and Southern Ocean upwelling, wind-sea surface interactions, NADW formation, deep ocean stratification, nutrient distributions and biological productivity (Morrison and Hogg, 2013; Ferrari et al., 2014; Jansen, 2017; Kohfeld and Chase, 2017; Marzocchi and Jansen, 2017). Furthermore, our linear application of the sea-ice proxy data of Wolff et al. (2010) to our air-sea gas exchange parameter may serve to overestimate its effect on the model results early in the glacial period (MIS 5d), and underestimate it during MIS 2-4 (Wolff et al., 2010).

Adkins et al. (2002) reconstructed LGM deep-sea salinity for the Southern, Atlantic and Pacific Oceans. They found increased salinity for the LGM at all locations, across a range of +0.95-2.4 practical salinity units (psu) above modern values,

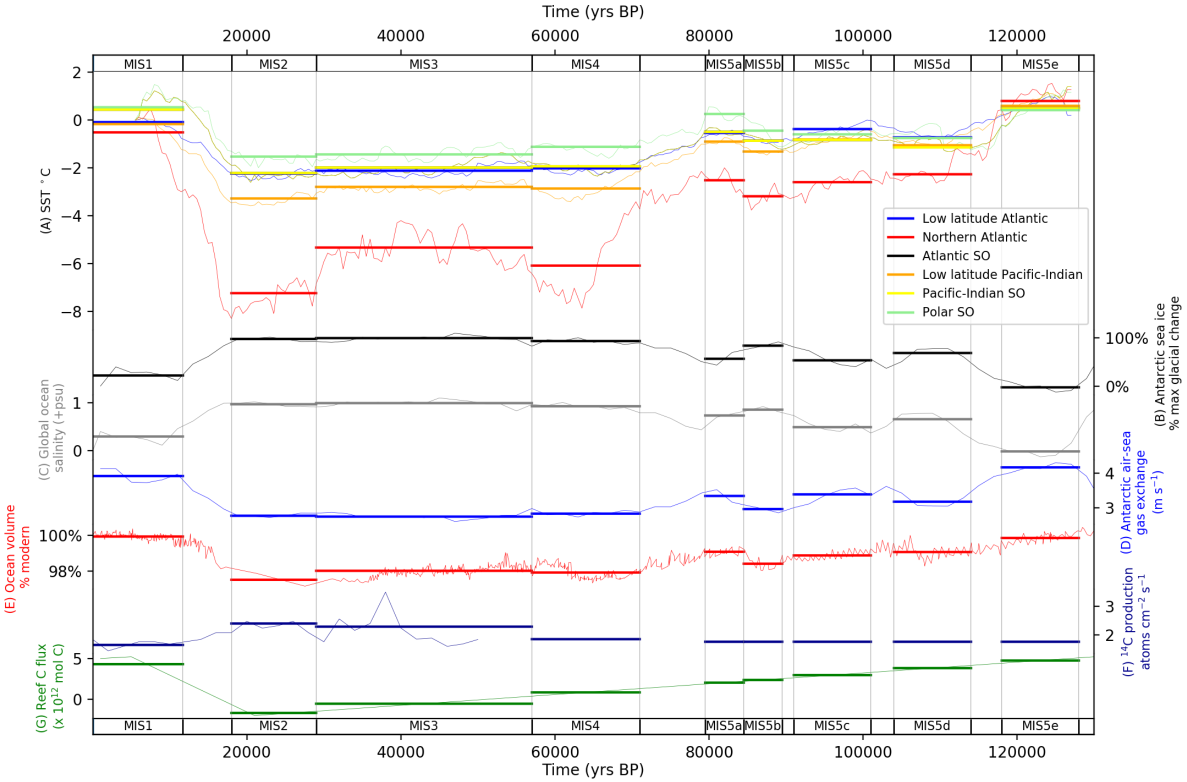

Figure 2. Model forcings for MIS across the last glacial cycle. (A) sea surface temperature reconstruction of (Kohfeld and Chase, 2017), mean values mapped into SCP-M surface boxes (fine lines) and averaged across MIS (bold lines). (B) Proxy for Antarctic sea-ice extent using ssNa fluxes from the EPICA Dome C ice core (Wolff et al., 2010), used to temporally contour MIS model forcings for (C) salinity (Adkins et al., 2002) and (D) polar Southern Ocean air-sea gas exchange. Global ocean salinity is forced to a glacial maximum of +1 psu (shown in (C)) and the polar Southern Ocean is forced to +2 psu (not shown), as modified from Adkins et al. (2002). Ocean volume (E) forced using global relative sea level reconstruction of Rohling et al. (2009). (F) Atmospheric ^{14}C production rate time series for 0-50 ka of Muscheler et al. (2014) . Long-term values assumed for >50 ka (Key, 2001). (G) Shallow water carbonate flux of carbon from Ridgwell et al. (2003) profiled across the glacial cycle using a curve from Opdyke and Walker (1992). Fine lines are the time series data and bold lines are the model forcings in each MIS. Data behind the figure are shown in Supplementary Information.

with an average value of +1.5 psu. The most saline LGM waters were in the Southern Ocean (+ 2.4 psu), with Atlantic and Pacific waters ranging +0.95-1.46 psu and an average of +1.2 psu. Adkins et al. (2002) also observed that within a (globally) more saline ocean, lower glacial temperatures would have caused less evaporation during the LGM, a negative feedback on salinity. We chose a global forcing for LGM sea surface salinity of +1 psu for the global ocean, and +2 psu for the polar Southern Ocean, relative to the interglacial period. These values conservatively reflect the hypothesis that surface evaporation may have been less in the LGM, hence a lesser magnitude of change in salinity in the surface ocean relative to the deep ocean values estimated by Adkins et al. (2002), and also that the most voluminous parts of the ocean were less saline than the Southern Ocean (Adkins et al., 2002). In our model-data experiments, the estimated glacial change in sea surface salinity (Fig. 2(C)), is also contoured through time with the variation in Antarctic sea-ice cover of Wolff et al. (2010). Adkins et al. (2002) observed that glacial salinity is a poor predictor of global mean sea level, due to storage of saline waters in ice shelves and groundwater reserves, hence the proxy for Antarctic sea-ice cover may have a more direct linkage to sea surface salinity than using global sea level, for our purposes of estimating temporal evolution in salinity.

Rohling et al. (2009) reconstructed global relative sea level (RSL) over the past five glacial cycles. According to Rohling et al. (2009), the glacial RSL minimum was $\sim$-115m at $\sim$27 ka, immediately prior to the LGM. We perform a simple calculation to reduce ocean depth and volume in SCP-M, in line with the Rohling et al. (2009) time series. In a box model this is only an approximation, given the lack of topographical detail. Varying ocean box volume and surface area, effects the ocean surface area available for in-gassing and de-gassing, and overall ocean capacity to store CO_2, which impacts atmospheric CO_2, $\delta^{13}C$ and $\Delta^{14}C$ (Köhler et al., 2010; O'Neill et al., 2019). Opdyke and Walker (1992) reconstructed coral reef carbonate fluxes of $CaCO_3$ for the last glacial cycle, for the purposes of modelling the "coral reef hypothesis". According to Opdyke and Walker (1992), reef carbon fluxes (out of the ocean) declined through the glacial cycle, with net dissolution in MIS 2 and MIS 3 leading to positive fluxes of carbon and alkalinity into the ocean in those periods. Fluxes of carbon and alkalinity out of the ocean into coral reefs, rebounded from the LGM (MIS 2) into the Holocene (MIS 1), driven by increased sea level and temperature (Kleypas, 1997). Given that Opdyke and Walker (1992) evaluated the possibility for coral reefs to drive the entire glacial-interglacial CO_2 variation, we have taken the more conservative modelling assumption of Ridgwell et al. (2003) of 0.5 x 10^{17} mol C, for postglacial accumulation of coral reefs. We have profiled this value across the glacial cycle accumulation/dissolution curve of Opdyke and Walker (1992), as shown in Fig. 2. We applied the estimated atmospheric production rate for ^{14}C for the last 50 kyr of Muscheler et al. (2014), with a long term average production rate of $\sim$1.7 atoms cm^{-2} s^{-1} assumed for 50-130 ka (Key, 2001).

The terrestrial biosphere module in SCP-M does not explicitly represent the carbon stored in buried peat, permafrost and also cold-climate vegetation that may have expanded its footprint in the glaciation, such as tundra biomes (e.g. Tarnocai et al., 2009; Ciais et al., 2012; Schneider et al., 2013; Eggleston et al., 2016; Ganopolski and Brovkin, 2017; Treat et al., 2019). The freezing and burial of organic matter across the glacial cycle may significantly imprint the terrestrial biosphere CO_2 size and $\delta^{13}C$ signature (Tarnocai et al., 2009; Ciais et al., 2012; Schneider et al., 2013; Eggleston et al., 2016; Ganopolski and Brovkin, 2017; Mauritz et al., 2018; Treat et al., 2019). Schneider et al. (2013) and Eggleston et al. (2016) both observed a permanent increase in atmospheric $\delta^{13}C$ during the last glacial cycle, of $\sim$0.4‰, and attributed its cause likely due to soil storage of carbon in peatlands which were buried or frozen as permafrost as the glacial cycle progressed. Ganopolski and Brovkin (2017) incorporated permafrost, peat, and buried carbon into their transient simulations of the last four glacial-interglacial cycles, observing that these features dampened the amplitude of glacial-interglacial variations in terrestrial biosphere carbon stock, in the CLIMBER-2 model. As a crude measure to account for this counter-CO_2 cycle storage of carbon in the terrestrial biosphere and frozen soils, we force the terrestrial biosphere productivity parameter in SCP-M in the range $\sim$+5-10 PgC yr^{-1}, increasing into the LGM (MIS 2), and maintained in the Holocene (MIS 1). We maintain the forcing of the terrestrial biosphere in the

Table 1. Free-floating parameter ranges in the model-data experiments, for global overturning circulation (Ψ_1), Atlantic meridional overturning circulation (Ψ_2) and Southern Ocean biological export productivity (Z). Parameters were varied simultaneously across these ranges and then optimised against proxy data in each MIS. Also shown are pre-industrial control values for GOC (Talley, 2013), AMOC (Talley, 2013) and Southern Ocean biological export productivity (Dunne et al., 2005; Sarmiento and Gruber, 2006; Henson et al., 2011; Siegel et al., 2014; DeVries and Weber, 2017). The Pacific-Indian Southern Ocean biology parameter is set at a base value of $\sim$70% Atlantic Southern Ocean box, but scales linearly with the Atlantic Ocean parameter in the experiments. The smaller values for Pacific-Indian Southern Ocean takes account of natural observations of a relatively stronger biological export productivity in the Atlantic sector of the subpolar Southern Ocean (e.g. Dunne et al., 2005; Sarmiento and Gruber, 2006; Henson et al., 2011; Siegel et al., 2014; DeVries and Weber, 2017).

Time period	**GOC (Ψ_1) Sv**	**AMOC (Ψ_2) Sv**	**Southern Atlantic (Pacific-Indian) Ocean biology (Z) mol C m^{-2} yr^{-1}**
PI control values	29	19	3.2 (2.2)
MIS experiment ranges	10-35	10-25	0.5-6.5 (0.3-4.5)

Holocene, as the posited effects of buried peat and permafrost storage of carbon on atmospheric CO_2 and $\delta^{13}C$ during the lead-up and into the LGM, were likely not fully reversed after the glacial termination (Tarnocai et al., 2009; Eggleston et al., 2016; Mauritz et al., 2018; Treat et al., 2019), and were partially or wholly replaced by other soil stocks of carbon (e.g. Lindgren et al., 2018). SCP-M calculates net primary productivity (NPP) using this productivity input parameter, as a function of carbon fertilisation (Harman et al., 2011).

$\sim$9,000 model simulations were undertaken across the parameter ranges in Table 1 for each MIS. Parameters were varied simultaneously to allow coverage of all possible combinations of the parameter values within their respective experiment ranges. Within these ranges, values are incremented by 1 Sv for GOC (Ψ_1) and AMOC (Ψ_2), and $\sim$0.5 mol C m^{-2} yr^{-1} for Atlantic Southern Ocean biological export productivity (Z). Each simulation was run for 10 kyr to enable the model to achieve steady state. We show the experiment ranges for the biological export productivity parameter Z for the Atlantic and Pacific-Indian sectors of the Southern Ocean (Table 1). In SCP-M, the Pacific-Indian Southern Ocean biological export productivity parameter (in mol C m^{-2} yr^{-1}) is set by default at a value of $\sim$70% of the corresponding Atlantic sector Southern Ocean box, to align with natural observations of variations in the Southern Ocean biological export productivity (e.g. Dunne et al., 2005; Sarmiento and Gruber, 2006; Henson et al., 2011; Siegel et al., 2014; DeVries and Weber, 2017). This variation is reflected in the values in Table 1. In the experiments, the values for Z in the Pacific-Indian Southern Ocean surface box scale linearly with the values for the Atlantic Southern Ocean surface box (Table 1). Herein we focus our presentation and discussion of the experiment results for the Z parameter on the Atlantic Southern Ocean, due to it's prominence in glacial cycle hypotheses for increased biological productivity (e.g. Martinez-Garcia et al., 2014; Lambert et al., 2015; Shaffer and Lambert, 2018; Muglia et al., 2018).

2.2.2 Optimisation procedure

We performed a least squares optimisation of the model experiment output against MIS data for atmospheric CO_2, atmospheric and deep and abyssal ocean Δ^{14}C and δ^{13}C, and deep and abyssal ocean carbonate ion proxy, to source the best-fit parameter values for GOC, AMOC and Southern Ocean biological productivity in each time slice - a brute force form of the *gradient descent* method for optimisation (e.g. Strutz, 2016). The equation for least fit applied was:

$$Opt_n = Min \sum_{i,k=1}^{N} (\frac{R_{i,k} - D_{i,k}}{\sigma_{i,k}})^2 \qquad (3)$$

where: Opt_n = optimal value of parameters *n* (e.g. GOC, AMOC and Southern Ocean biological productivity), $R_{i,k}$ = model output for concentration of each element *i* in box *k*, $D_{i,k}$ = average data concentration each element *i* in box *k* and $\sigma_{i,k}$ = standard deviation of the data for each element *i* in box *k*. The standard deviation performs two roles. It normalises for different unit scales (e.g. ppm, ‰ and μmol kg^{-1}), which allows multiple proxies to be incorporated in the optimisation, and reduces the weighting of a proxy data point with a high standard deviation, and therefore an uncertain value. The weighting by proxy data standard deviation also fulfils the important role of accounting for data variance in the optimised parameter results, such that the effects of data variance are embedded in the optimised parameter values. Where proxy data is unavailable for a box, that data and box combination is automatically omitted from the optimisation routine. The experiment routine returns the model run with the best fit to the data, and the model's parameters and results.

2.3 Data

The model-data optimisation rests on compilations of atmospheric and ocean paleo proxy data. We compile and apply published proxy data for atmospheric CO_2, δ^{13}C and Δ^{14}C and ocean δ^{13}C, Δ^{14}C and carbonate ion. Sources of proxy data are shown in Table 2 and data locations in Fig. 3.

2.3.1 Ocean carbon isotopes

We gathered published marine Δ^{14}C data extending back to ~40 ka (Table 2). Our dataset incorporates individual records contributed over the last ~thirty years and supplemented by the recent compilations of Skinner et al. (2017) and Zhao et al. (2017). The data total ~75 individual location estimates for benthic and planktonic foraminifera, and deep sea corals. We have restricted our efforts to time series which contain independent calendar ages, and therefore corrections for radioactive decay in the time since the sample was deposited (yielding Δ^{14}C). Figure 3 shows the geographic distribution of the Δ^{14}C data, which is generally concentrated on ocean basin margins. Some regions, such as the central Pacific, southern Indian and polar Southern Ocean, are devoid of data.

Table 2. Ocean and atmosphere proxy data sources for the last glacial-interglacial cycle

Indicator	**Time period coverage**	**Reference**
Atmosphere CO_2	0-800 ka	Bereiter et al. (2015)
Atmosphere $\delta^{13}C$	0-155 ka	Eggleston et al. (2016)
Atmosphere $\Delta^{14}C$	0-50 ka	Reimer et al. (2009)
Ocean $\delta^{13}C$	0-120 ka	Oliver et al. (2010), Govin et al. (2009), Piotrowski et al. (2009)
Ocean $\Delta^{14}C$	0-40 ka	Skinner and Shackleton (2004), Marchitto et al. (2007), Barker et al. (2010), Bryan et al. (2010), Skinner et al. (2010), Burke and Robinson (2012), Davies-Walczak et al. (2014), Skinner et al. (2015), Chen et al. (2015), Hines et al. (2015), Sikes et al. (2016), Ronge et al. (2016), Skinner et al. (2017), Zhao et al. (2017)
Ocean carbonate ion proxy	0-705 ka	Yu et al. (2010), Yu et al. (2013), Yu et al. (2014b), Yu et al. (2014a), Broecker et al. (2015), Yu et al. (2016), Qin et al. (2017), Qin et al. (2018), Chalk et al. (2019)

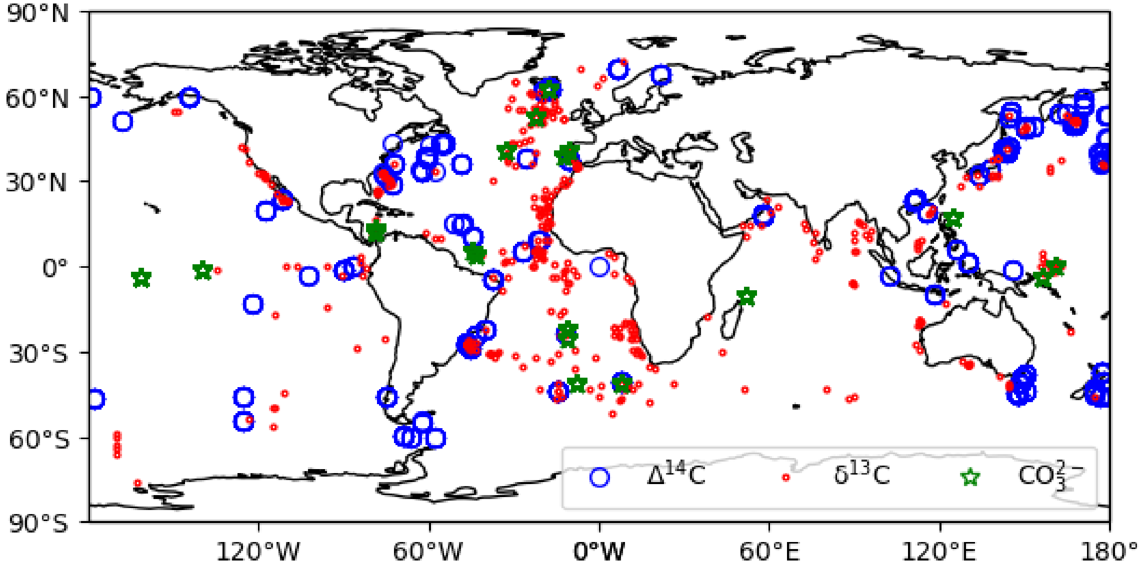

Figure 3. $\Delta^{14}C$, $\delta^{13}C$ and CO_3^{2-} data locations. $\Delta^{14}C$ and CO_3^{2-} data was compiled from published estimates. For $\delta^{13}C$ we take the compilation of Oliver et al. (2010).

Oliver et al. (2010) compiled a global dataset of 240 cores of marine δ^{13}C data encompassing benthic and planktonic species over the last $\sim$150 kyrs. Oliver et al. (2010) observed considerable uncertainties associated with the broad range of species included, particularly for the planktonic foraminifera. By comparison, Peterson et al. (2014) aggregated marine δ^{13}C for the LGM and late Holocene periods, as time period averages, exclusively sampling benthic *C. wuellerstorfi* data, which is a more reliable indicator of marine δ^{13}C (Oliver et al., 2010; Peterson et al., 2014). To narrow the range of uncertainty, we constrain our use of marine δ^{13}C data to the deep and abyssal (>2,500m) benthic *Cibicides* species foraminifera samples in the Oliver et al. (2010) dataset, supplemented with *Cibicides* species δ^{13}C proxy data from Govin et al. (2009) and Piotrowski et al. (2009) (Table 2). Figure 3 shows the δ^{13}C data locations from Oliver et al. (2010), which are concentrated in the Atlantic Ocean. We mapped and averaged the carbon isotope data into SCP-M's boxes on depth and latitude coordinates (Fig. 1), and averaged for each MIS time slice.

2.3.2 Carbonate ion proxy

We aggregated ocean carbonate ion proxy data from the sources shown in Table 2 and locations in Fig. 3, mapped into SCP-M box coordinates and averaged the data across MIS. The data coverage for CO_3^{2-} is relatively sparse, with <20 individual site locations across the global ocean. However, the depth and lateral coverage of SCP-M's boxes is large, particularly in the case of the deep ocean boxes, which cover the full lateral extent of the Pacific-Indian and Atlantic oceans, and depth ranges of 100-2,500m (Pacific-Indian) and 250-2,500m (Atlantic). CO_3^{2-} can vary by more than 100 μmol kg^{-1} across the depth range 100-2,500m, and can vary by up to $\sim$200 μmol kg^{-1} in the shallow ocean (e.g. Sarmiento and Gruber, 2006; Yu et al., 2014b, a). Some boxes contain only one core, creating an exceptionally low standard deviation range relative to the other proxies. In other cases, such as the deep Atlantic ocean, the data points are clustered within the 2,000-2,500m depth range, the bottom third of the corresponding SCP-M box. This clustering becomes a problem for the SCP-M box model, which outputs average concentrations over the complete depth range of each box - a drawback of using a large resolution box model to analyse proxy data at a global ocean level. Furthermore, the very low standard deviations associated with the CO_3^{2-} data (data shown in Supplementary Information) cause it to assume a disproportionate weighting in the model-data optimisation, which uses standard deviation for weighting of proxies, relative to ocean δ^{13}C and Δ^{14}C. The latter proxies often have box standard deviations up to 100% of their mean value, when averaged across a box. This issue is also an artefact of our procedure necessary to normalise the different proxies (each in unique units) in a multi-proxy model-data optimisation, by using the standard deviation as a weighting. To deal with this, we have assigned an arbitrary standard deviation (weighting) of 15 μmol kg^{-1} to CO_3^{2-} data observations in our model-data optimisations, which acts as a feasible weighting for the processing of the CO_3^{2-} relative to the other ocean proxy data. This value is a small fraction of the variation in CO_3^{2-} concentrations observed over the depth range 100-2,500m in the modern ocean (e.g. Key et al., 2004; Yu et al., 2014b).

3 Data analysis

Figure 4 shows the atmospheric data used to constrain the model, averaged into MIS time slices. There are many fluctuations and transient changes, but three major sustained reductions in atmospheric CO_2 in the lead-up to the LGM (Fig. 4(A)). A drop of ∼25 ppm in MIS 5d, a further drop of ∼30 ppm in MIS 4, and finally a fall of ∼20 ppm in the period leading up to the LGM (between MIS 2 and 4). These are the three major CO_2 events described in Kohfeld and Chase (2017), and, combined with additional reductions of ∼-10 ppm throughout the period, yield a total drop of ∼-85 ppm from the penultimate interglacial to the LGM. Transient changes in atmospheric CO_2 are littered throughout the glacial cycle, including in MIS 5b, MIS 4 and throughout MIS 3. CO_2 increases by ∼85 ppm in the glacial termination and Holocene periods.

Atmospheric δ^{13}C (Fig. 4(B)) increased by ∼0.4‰ between the penultimate interglacial (MIS 5e) and the Holocene (MIS 1), with temporary falls at MIS 5d, MIS 4 and in the last glacial termination (between MIS 1 and 2). The cause of the observed increase in atmospheric δ^{13}C across the last glacial-interglacial cycle may be the effect of accumulation and freezing, or burial in glacial sediments, of peat and other soil organic matter at the high latitudes (e.g. Tarnocai et al., 2009; Ciais et al., 2012; Schneider et al., 2013; Eggleston et al., 2016; Ganopolski and Brovkin, 2017; Treat et al., 2019). According to Treat et al. (2019), peatlands and other vegetation accumulated carbon in the relatively warm periods, and these carbon stocks were then frozen and/or buried in glacial and other sediments during the cooler periods, throughout the last glacial cycle. This buried or frozen stock of carbon persists to the present day (Tarnocai et al., 2009), although according to Ciais et al. (2012) it may be smaller now than in the LGM. Schneider et al. (2013) evaluated several possible candidates for the rising atmospheric δ^{13}C pattern across the last glacial-interglacial cycle and could not discount any of (1) changes in the carbon isotope fluxes of carbonate weathering and sedimentation on the seafloor, (2) variations in volcanic outgassing or (3) peat and permafrost build-up throughout the last glacial-interglacial cycle.

The large drop in δ^{13}C in MIS4, reverses in MIS 3 (Fig. 4(B)). This excursion in the δ^{13}C pattern likely resulted from sequential changes in SST (cooling), AMOC, Southern Ocean upwelling and marine biological productivity (Eggleston et al., 2016). Eggleston et al. (2016) parsed the atmospheric δ^{13}C signal into its component drivers across MIS 3-5, using a stack of proxy indicators, and highlighted the sequence of events between the end of MIS 5 and beginning of MIS 3, and their cumulative effects to deliver the full change in atmospheric δ^{13}C. Our MIS-averaging approach fails to capture the full amplitude of the changes in atmospheric δ^{13}C during MIS 3-5, and only captures the changes in the mean-MIS value, serving to understate the full extent of transient changes in responsible processes. In addition, the MIS-averaging approach misses the sequential timing of changes in processes within each MIS. These are limitations of our steady-state, MIS-averaging approach. The reduction in atmospheric δ^{13}C at the last glacial termination, between MIS 1 and MIS 2, coincident with a large atmospheric CO_2 increase, is attributed to the release of deep-ocean carbon to the atmosphere resulting from increased ocean circulation and Southern Ocean upwelling (Schmitt et al., 2012). The subsequent rebound of δ^{13}C in the termination period and the Holocene is believed to result from terrestrial biosphere regrowth, in response to increased CO_2 and carbon fertilisation (Schmitt et al., 2012; Hoogakker et al., 2016).

The atmospheric $\Delta^{14}C$ data covers the period 0-50ka (Reimer et al., 2009). During this period, $\Delta^{14}C$ is heavily influenced by declining atmospheric ^{14}C production (Broecker and Barker, 2007; Muscheler et al., 2014). In addition, an acceleration in atmospheric $\Delta^{14}C$ decline at the last glacial termination is attributed to the release of old, ^{14}C-depleted waters from the deep ocean, due mainly to increased Southern Ocean upwelling (e.g. Sikes et al., 2000; Marchitto et al., 2007; Skinner et al., 2010; Burke and Robinson, 2012; Siani et al., 2013; Skinner et al., 2017).

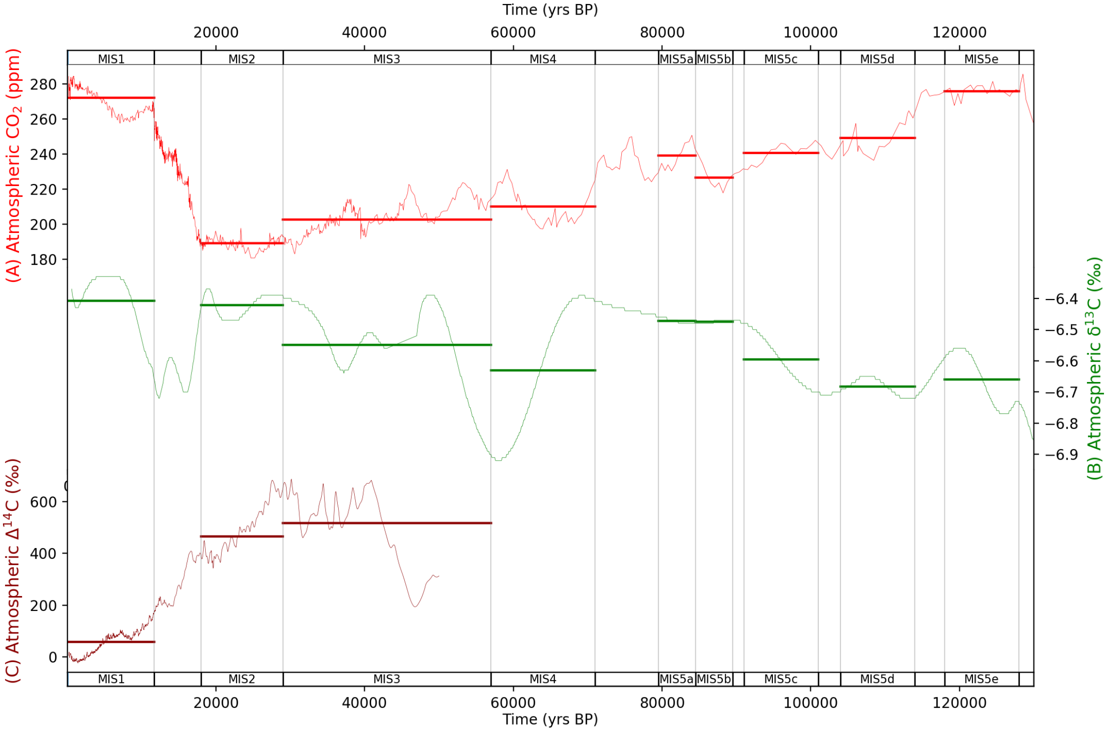

Figure 4. MIS atmosphere data for (A) atmospheric CO_2 (Bereiter et al., 2015), (B) $\delta^{13}C$ (Eggleston et al., 2016) and (C) $\Delta^{14}C$ (Reimer et al., 2009). Data are shown in fine lines, with bold horizontal lines for MIS-sliced data. Natural observations for $\Delta^{14}C$ do not exist beyond $\sim$50 ka due to the radioactive decay of ^{14}C. Data behind the figure are shown in Supplementary Information.

Figure 5 shows deep and abyssal ocean $\delta^{13}C$ data mapped into SCP-M box model space and averaged across MIS. The visual offset between deep and abyssal proxy data values is regularly interpreted as an indicator of the strength of deep ocean circulation and/or mixing, or biological productivity, during the LGM and the Holocene (e.g. Sikes et al., 2000; Curry and Oppo, 2005; Marchitto et al., 2007; Oliver et al., 2010; Skinner et al., 2010; Burke and Robinson, 2012; Yu et al., 2013, 2014a; Skinner et al., 2015, 2017). The deep-abyssal Atlantic $\delta^{13}C$ time series (Fig. 5(A)) exhibits modest widening in the deep and abyssal offset between MIS 5d and 5e, again at MIS 5b, and a more substantial widening at MIS 4 and at MIS 2 (the LGM). The widening of the offset during MIS 2-4 is caused primarily by more negative abyssal $\delta^{13}C$ values. The offset is almost closed in MIS 1 (the Holocene). The deep Atlantic $\delta^{13}C$ range itself also widens considerably from MIS 4, and narrows after the LGM. Oliver et al. (2010) and Kohfeld and Chase (2017) interpreted these patterns as the result of weakened deep Atlantic ocean circulation at MIS 4 and at the LGM, rebounding in the post glacial period.

The Pacific-Indian δ^{13}C data (Fig. 5(B)) shows a drop in abyssal δ^{13}C and widening in the deep-abyssal offset at MIS 5d, continuing throughout the last glacial cycle. Importantly, the more negative abyssal δ^{13}C values during MIS 5a-5d, occur at the same time that atmospheric δ^{13}C becomes more positive (Fig. 4(B)), suggesting that the abyssal Pacific-Indian ocean became more isolated from the atmosphere during this period. This is qualitative evidence for slowing ocean circulation or increased biological export productivity in the Pacific-Indian ocean, at that time. This also corresponds with a ∼35 ppm fall in CO_2 across MIS 5a-5e (Fig. 4(A)). Abyssal Pacific-Indian δ^{13}C drops further and most noticeably at MIS 4, and again at the LGM, and then rebounds from the LGM into the Holocene period, as also observed in the Atlantic Ocean δ^{13}C data. Statistical analysis of the δ^{13}C data, provided in the Supplementary Information (Fig. S1 and Table S8), supports our qualitative interpretation of the data.

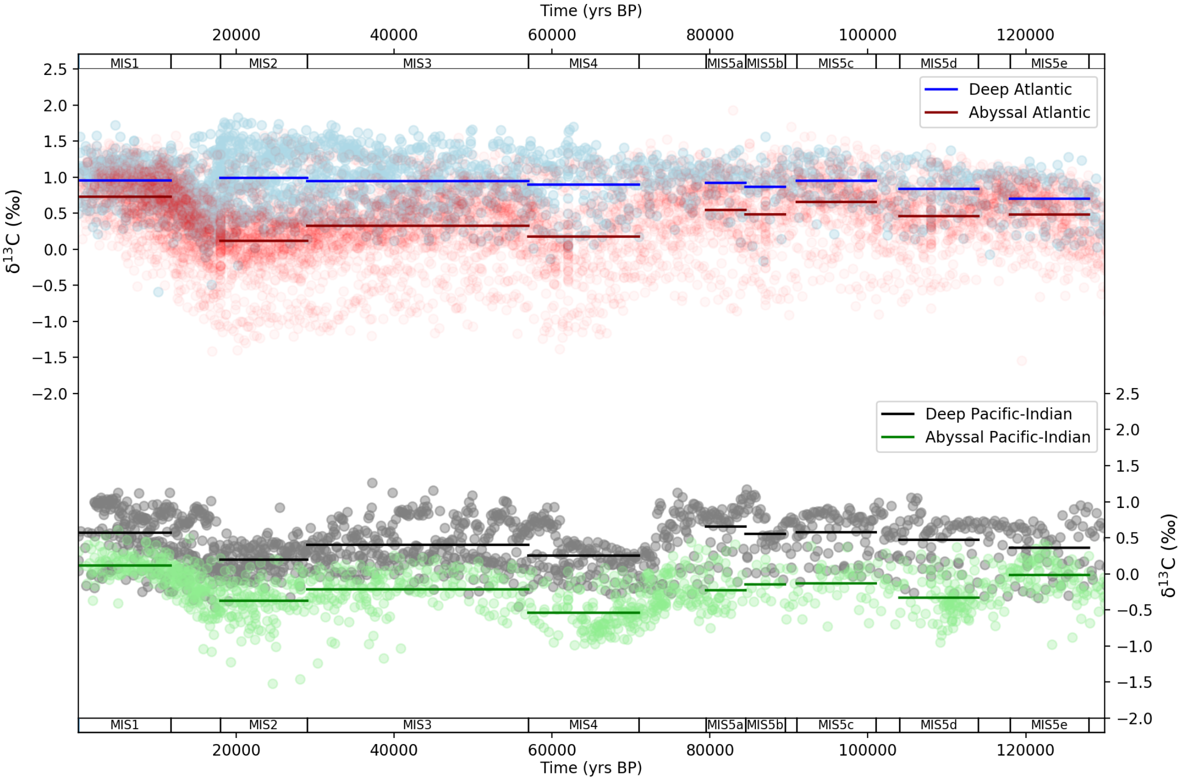

Figure 5. MIS ocean data mapped into SCP-M box model dimensions for δ^{13}C (Oliver et al., 2010). Data (round circles) are mapped into deep (2,500m average depth) and abyssal (3,700 (Atlantic) - 4,000m (Pacific-Indian) average depth) model boxes and averaged across MIS slices (bold lines). Data behind the figure are shown in Supplementary Information.

Ocean Δ^{14}C data covers the MIS 1-3 periods, and the LGM and Holocene in most detail (Fig. 6). We show ocean $\Delta\Delta^{14}$C, which is atmospheric less ocean Δ^{14}C. This calculation is made in attempt to normalise the effects of varying atmospheric ^{14}C production through the glacial cycle (Broecker and Barker, 2007; Muscheler et al., 2014), which imparts a dominant influence on the ocean Δ^{14}C trajectory. Given the sparse data coverage for MIS 3, we focus our analysis on MIS 1 and 2. The $\Delta\Delta^{14}$C time series exhibits two key features across the LGM (MIS 2) and Holocene periods (MIS 1). First, there is a narrowing in the spread of values between the shallow and abyssal ocean from the LGM to the Holocene, in both the Atlantic (Fig. 6(A)) and Pacific-Indian (B) basins. Second, all ocean boxes display an increase in $\Delta\Delta^{14}$C from the LGM to the Holocene, towards equilibrium with the atmosphere. These patterns are believed to represent increased overturning circulation in the Atlantic and Pacific-Indian basins across the LGM-Holocene. Increased ocean overturning brought old, Δ^{14}C-negative water up from the deep and abyssal oceans, mixing with shallow and intermediate waters, and eventually into contact with the atmosphere, where ^{14}C is produced - known as "increased ventilation" (e.g. Sikes et al., 2000; Marchitto et al., 2007; Bryan et al., 2010; Skinner et al., 2010; Burke and Robinson, 2012; Davies-Walczak et al., 2014; Skinner et al., 2014; Hines et al., 2015; Freeman et al., 2016; Sikes et al., 2016; Skinner et al., 2017).

The Atlantic ocean CO_3^{2-} time series shows a similar pattern to $\Delta\Delta^{14}$C and δ^{13}C, with a wide dispersion of shallow-abyssal and deep-abyssal concentrations at the LGM, which narrows at the Holocene (Fig. 7). This pattern has been interpreted as varying strength and/or depth of AMOC and biological productivity in the Atlantic Ocean (e.g. Yu et al., 2013, 2014b, a, 2016). The abyssal Atlantic CO_3^{2-} pattern, which spans the last glacial cycle, is punctuated by two downward excursions (Fig. 7). These occur at MIS 4 and MIS 2, corresponding to the second major atmospheric CO_2 drop in the glacial cycle, and the LGM, respectively. The lower CO_3^{2-} value at MIS 4 was interpreted by Yu et al. (2016) as shoaling of AMOC and increased carbon storage in the deep-abyssal Atlantic Ocean. This signal is repeated at the LGM, where further shoaling and slowing AMOC contributed to deep oceanic drawdown of CO_2 from the atmosphere (Yu et al., 2013, 2014b, a). There is a modest drop in abyssal Atlantic Ocean CO_3^{2-} at MIS 5b (-13 μmol kg^{-1} relative to MIS 5c), which coincides with a minor drop in abyssal Atlantic Ocean δ^{13}C (-0.19‰) and atmospheric CO_2 (-14 ppm), indicating a common link. Menviel et al. (2012) modelled a transient slowdown in North Atlantic overturning circulation for this period, which could explain these features.

The Pacific Ocean is thought to partially buffer the effects of ocean circulation on CO_3^{2-} concentrations (Fig. 7) via changes in shallow (reef) and deep carbonate production and dissolution, and therefore displays less variation across the MIS (Yu et al., 2014b; Qin et al., 2017, 2018). The deep and abyssal Pacific-Indian ocean data shows a gradual trend of increasing CO_3^{2-} through the glacial cycle (Fig. 7), suggesting that it is influenced by variations in shallow and deep sea carbonate production and dissolution, and less by deep ocean circulation (Yu et al., 2014b; Qin et al., 2017, 2018). Notable exceptions are MIS 5d and MIS 4. At MIS 5d, both deep and abyssal Pacific-Indian ocean CO_3^{2-} drop (Fig. 7), aligning with the contemporary drop in abyssal δ^{13}C and atmospheric CO_2 (Fig. 5 and Fig. 5(B)), suggesting a possible common driver, and providing additional qualitative evidence for changes in either Pacific-Indian ocean circulation or biology, at this time. At MIS 4, there is a drop in deep Pacific-Indian CO_3^{2-} and a modest widening in the deep-abyssal offset from prior periods, also suggestive of the influence of deep ocean circulation and/or biological export productivity (Fig. 7). The widest Pacific-Indian deep-abyssal offset CO_3^{2-} is observed in MIS 3, also seen in the δ^{13}C and $\Delta\Delta^{14}$C data (Figs 5-7), indicating it is a persistent feature of the proxy records,

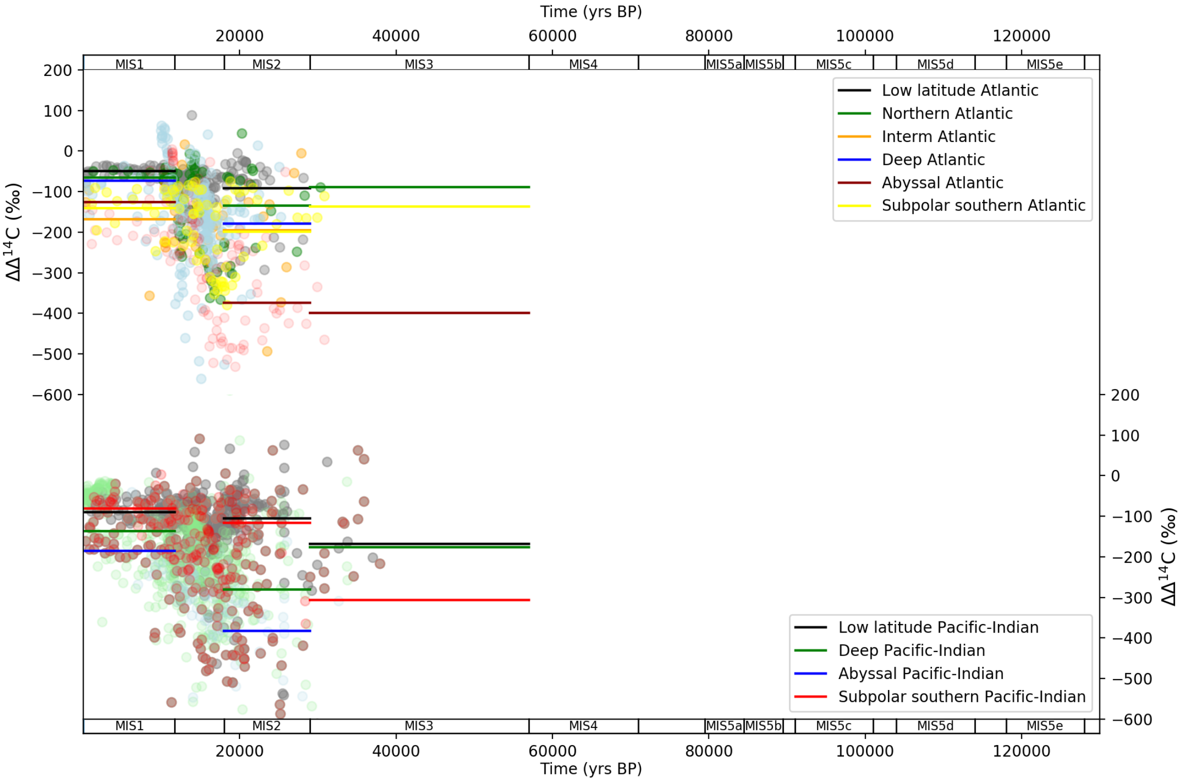

Figure 6. MIS stage ocean data mapped into box model dimensions for $\Delta\Delta^{14}$C. Data (round circles) are mapped into deep (2,500m average depth) and abyssal (3,700 (Atlantic) - 4,000m (Pacific-Indian) average depth) model boxes and averaged across MIS slices (bold lines). Natural observations do not exist beyond ∼50 ka due to the radioactive decay of ^{14}C. Data behind the figure are shown in Supplementary Information.

and suggesting MIS 3 may be the nadir of Pacific-Indian ocean circulation and/or the peak in biological activity in the glacial cycle, and at least that most changes in this part of the ocean took place prior to the LGM.

4 Results

Figure 8 shows the data-optimised values returned from the model-data experiments for GOC, AMOC and Atlantic Southern Ocean biological productivity parameters, in each MIS ("X" symbols). The optimised values take account of data variance, due to the weighting of proxy data points by their standard deviation in the model-data optimisation equation (Eq. 3). The full range of model-data experiment results are shown in the Supplementary Information. The GOC parameter (Ψ_1) value falls from 29 Sv to 22 Sv between MIS 5e and 5d, with gradual declines during MIS 5a-5c and a slight acceleration in the rate of decline during MIS 3-4. GOC reaches it’s minimum glacial value (16 Sv) in MIS 3, maintained in MIS 2 (LGM), and

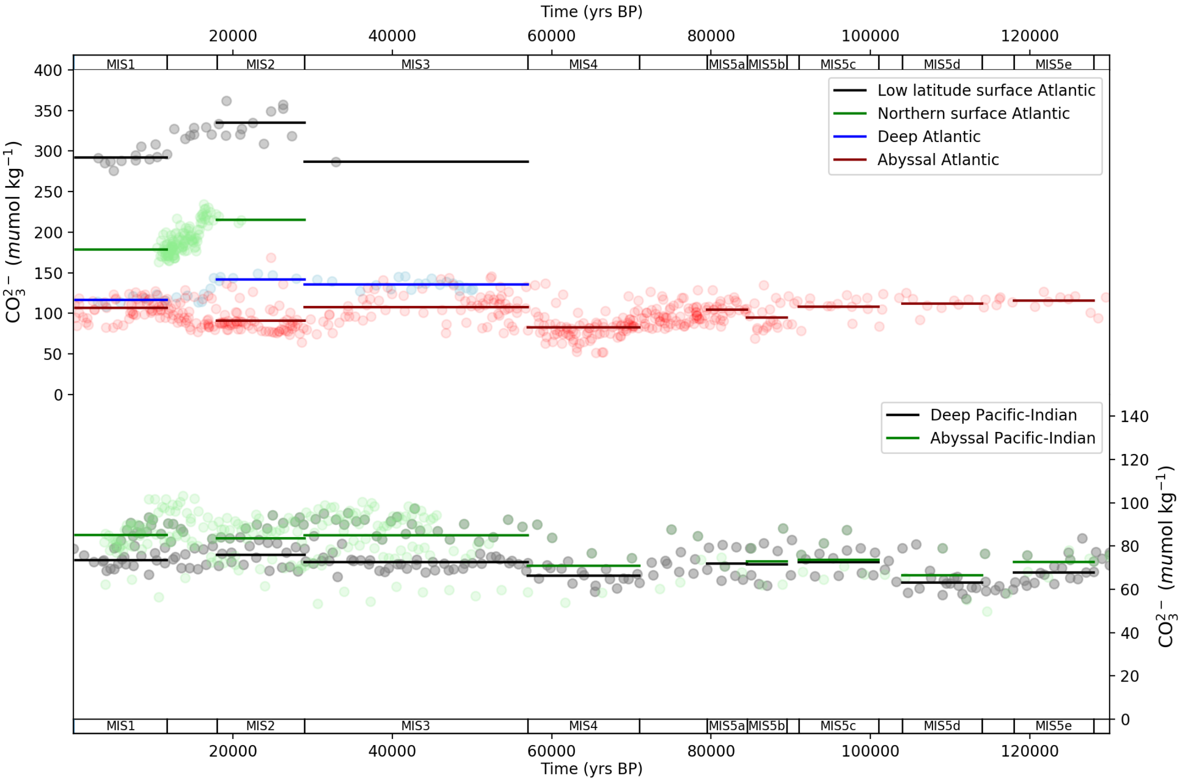

Figure 7. MIS stage ocean data mapped into box model dimensions for carbonate ion proxy. Data (round circles) are mapped into deep Data (round circles) are mapped into deep (2,500m average depth) and abyssal (3,700 (Atlantic) - 4,000m (Pacific-Indian) average depth) model boxes and averaged across MIS slices (bold lines). and abyssal (3,700 (Atlantic) - 4,000m (Pacific-Indian) average depth) model boxes and averaged across MIS slices (bold lines). Data behind the figure are shown in Supplementary Information.

then increases to 31 Sv in MIS 1. AMOC (Ψ_2) weakens modestly in MIS 5d, with a larger drop at MIS 5b that is partially reversed in MIS 5a. AMOC weakens further in MIS 4, achieving its glacial nadir, which is maintained until the LGM, before increasing to 18 Sv in MIS 1. Importantly, Ψ_2 closely follows the abyssal Atlantic δ^{13}C and CO_3^{2-} data pattern across the glacial cycle, and $\Delta\Delta^{14}$C from the LGM to the Holocene (Figs 5-7). Ψ_2 remains near it's modelled penultimate interglacial value (MIS 5e, 18 Sv), during MIS 5c and 5d, before dropping in MIS 5b (abyssal Atlantic δ^{13}C and CO_3^{2-}, and atmospheric CO_2, also drop at this point), before partly rebounding at MIS 5a and then falling synchronously with abyssal Atlantic δ^{13}C and CO_3^{2-} concentrations during MIS 2-4. Southern Ocean biological export productivity (Z) fluctuates around its penultimate interglacial (MIS 5e) value during MIS 5a-5d, then increases during MIS 4. Atlantic (Pacific-Indian) Southern Ocean Z spikes to 4.7 (3.3) mol C m^{-2} yr^{-1} in the LGM, then falls to 3.8 (2.6) mol C m^{-2} yr^{-1} in MIS 1.

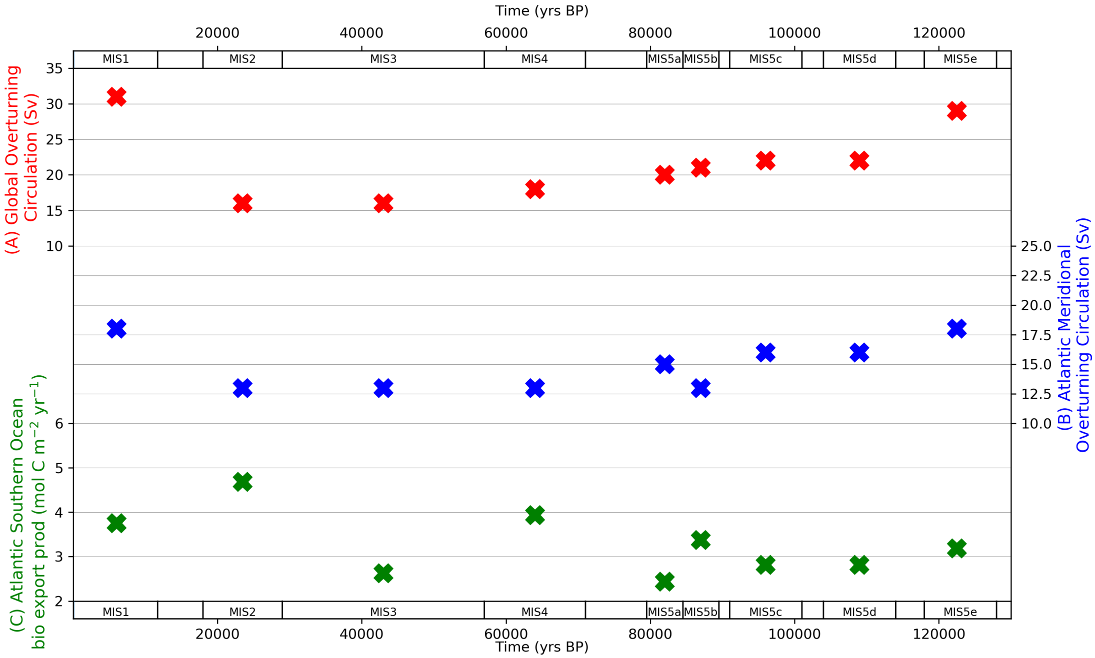

Figure 8. Model-data experiment results for global overturning circulation (A), Atlantic meridional overturning circulation (B) and Atlantic Southern Ocean biological export productivity (C). "X" symbols mark the optimal parameter values returned from the model-data experiments. The optimised values take account of data variance, due to the weighting of proxy data points by their standard deviation in the model-data optimisation equation (Eq. 3). Data for optimised parameter values shown in the figure are contained in Supplementary Information.

Figure 9 show the optimised model-data output for atmospheric CO_2 and ocean carbonate ion proxy, compared with the data observations, in each MIS. This shows how well the model is constrained by the proxy data, and also how well the model-data output of parameter values can explain the proxy data patterns as described in the data analysis section. The model-data results fall within one standard deviation of atmospheric CO_2 and deep and abyssal CO_3^{2-} data, and mostly on the MIS means, across the MIS periods (Fig. 9). The modelled abyssal Pacific-Indian CO_3^{2-} falls close to the MIS proxy data means across the glacial-interglacial cycle, but misses some of the variations in the data - particularly across MIS 3-4 (Fig. 9). This is a result of the abyssal ocean box carbonate dissolution equations in SCP-M, which effectively buffer any changes in the relative balance of DIC and alkalinity from ocean physical and biological changes, and possibly the large box sizes in SCP-M, which misses some detail for CO_3^{2-}.

The model-data results show good agreement with atmospheric, deep and abyssal δ^{13}C data throughout the MIS (Fig. 10). The results mostly fall on the mean and all are within the standard deviation for atmospheric δ^{13}C data in the MIS. All results

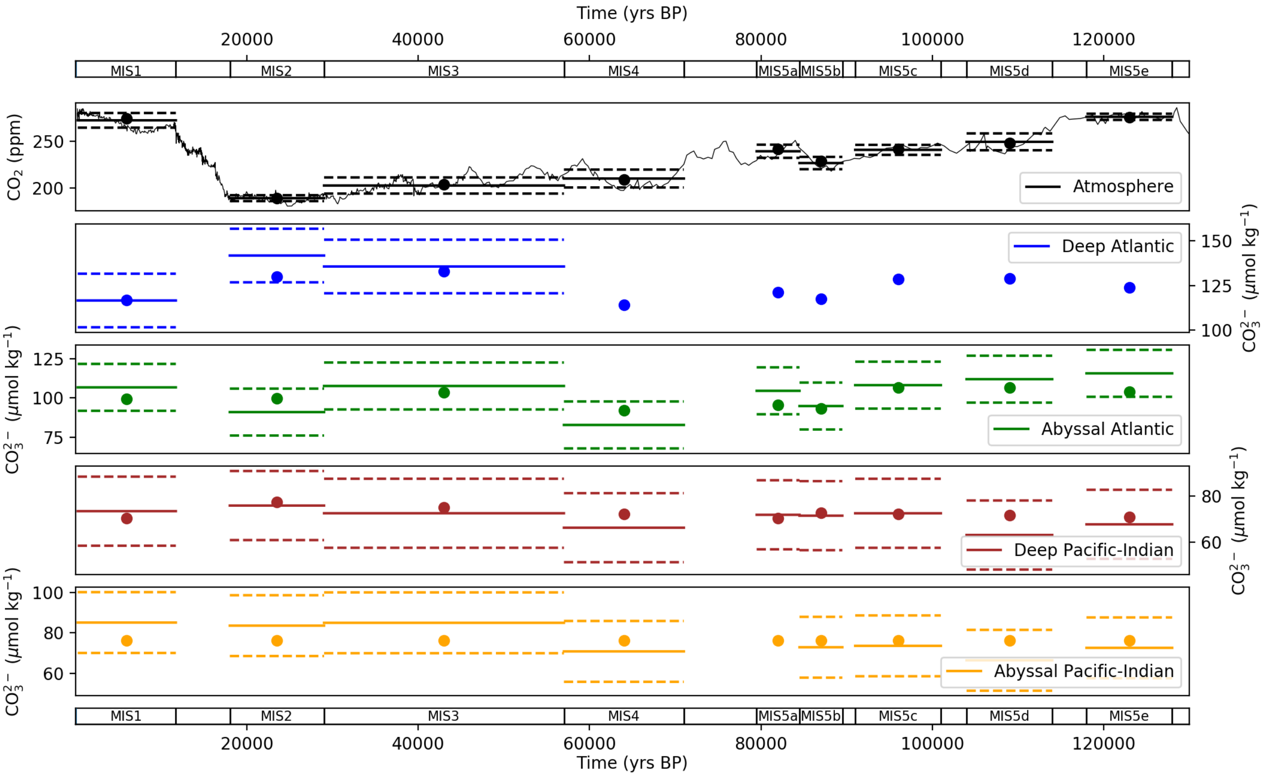

Figure 9. Values returned from the model-data experiment for (A) atmospheric CO_2 and carbonate ion proxy for (B) deep Atlantic (2,500m average depth), (C) abyssal Atlantic (3,700m average depth), (D) deep Pacific-Indian (2,500m average depth) and (E) abyssal Pacific-Indian (4,000m average depth). Model-data experiment results are shown as dots, with mean proxy data shown as solid lines, and one standard deviation range by dashed lines, in each MIS. A default standard deviation of 15 μmol kg^{-1} is used as discussed in the text. CO_3^{2-} data for the SCP-M deep Atlantic box in (B) does not extend beyond 50 ka.

fall within standard deviation for the deep and abyssal Atlantic and Pacific-Indian oceans. The modelled abyssal Pacific-Indian box δ^{13}C underestimates mean MIS δ^{13}C in most MIS time slices, which may reflect a discrepancy between the average depth of the δ^{13}C proxy data and SCP-M abyssal ocean box, or a bias in the model's equations.

Figure 11 shows model-data results for atmospheric Δ^{14}C and ocean $\Delta\Delta^{14}$C compared with data, for MIS 1-3. Model-data results fall within one standard deviation of the data for all observations that were modelled, and replicate the dramatic compression in deep-abyssal $\Delta\Delta^{14}$C and ocean-atmosphere offsets, between MIS 2 (LGM) and MIS 1 (the Holocene) as shown in the data (Fig. 11).

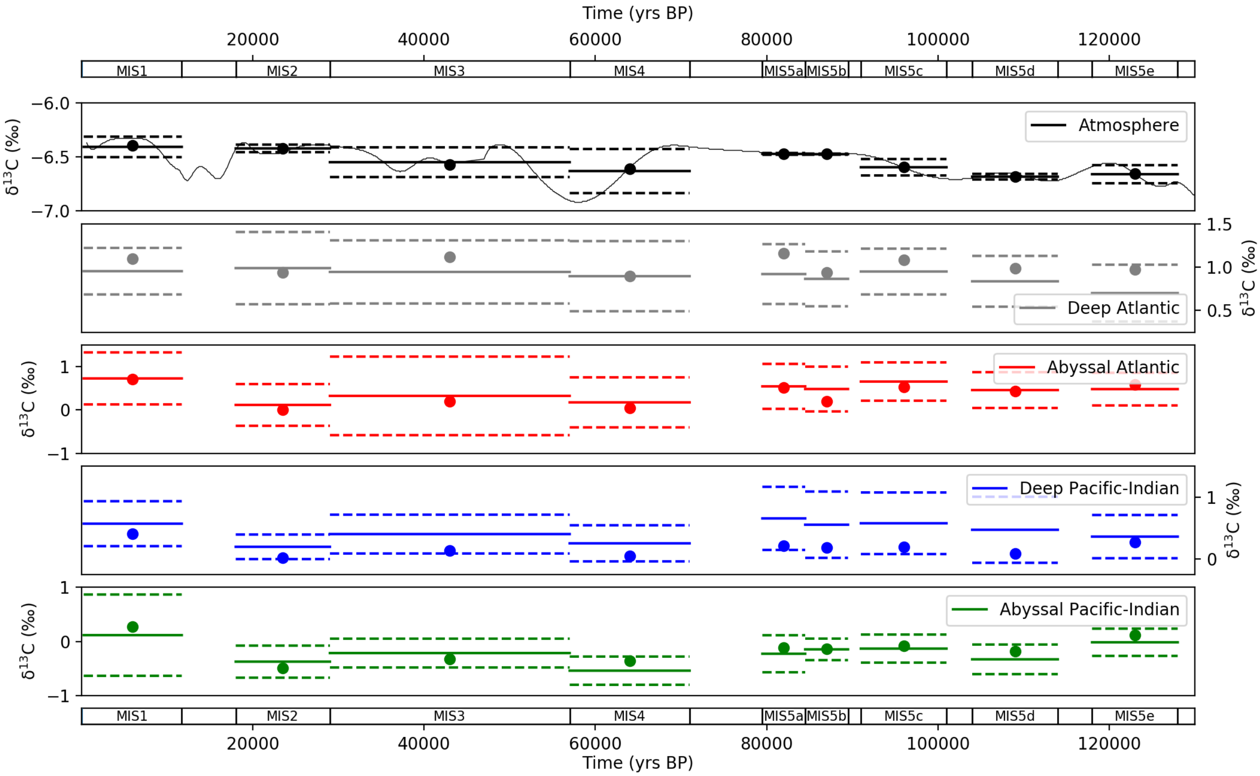

Figure 10. Values returned from the model-data experiment for $\delta^{13}C$ for (A) atmosphere, (B) deep Atlantic (2,500m average depth), (C) abyssal Atlantic (3,700m average depth), (D) deep Pacific-Indian (2,500m average depth) and (E) abyssal Pacific-Indian (4,000m average depth). Model-data experiment results are shown as dots, with proxy data mean (solid lines) and one standard deviation (dashed lines) in each MIS.

Figure 12 shows model-data output for the terrestrial biosphere net primary productivity (NPP) and carbon stock during the last glacial-interglacial cycle. The NPP and carbon stock follow atmospheric CO_2 down in the lead-up to the LGM and rebound from the LGM to the Holocene. This is the effect of carbon fertilisation (Harman et al., 2011; Hoogakker et al., 2016). Notably, there is a distinct drop in NPP at MIS 4, a period where atmospheric CO_2 falls by ∼30 ppm (Fig. 4(A)). Hoogakker et al. (2016) provided a reconstruction of NPP through the glacial cycle using pollen data and climate models, shown for comparison in Fig. 12(A). Our model-data results for NPP periodically fall in the upper and lower end, but within of the range of values from the Hoogakker et al. (2016) compilation, with the exception of MIS 5e where our results likely underestimate those of Hoogakker et al. (2016) (which extend only to 120 ka). We model the terrestrial biosphere carbon stock to fall by ∼400 PgC from the penultimate interglacial to the LGM, and increase by ∼630 PgC from the LGM to the Holocene (Fig. 12(B)).

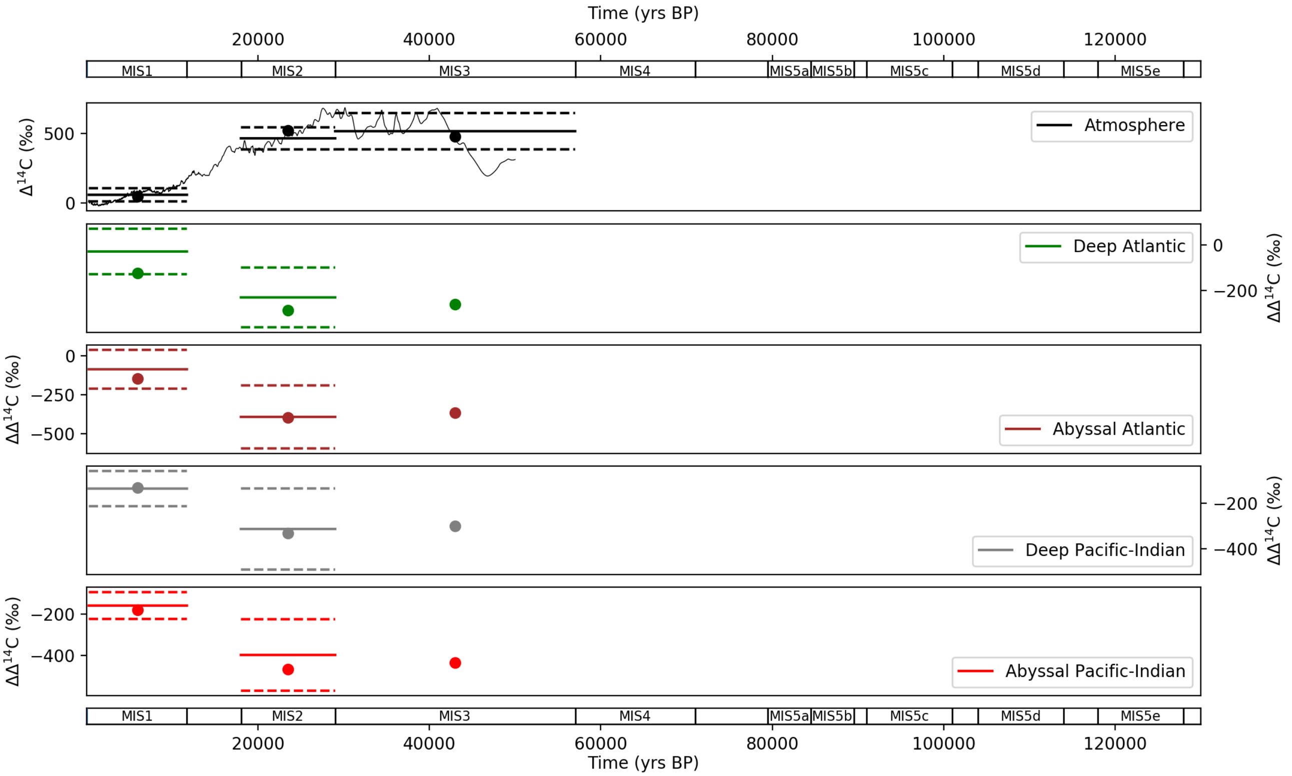

Figure 11. Values returned from the model-data experiment for (A) atmospheric Δ^{14}C and $\Delta\Delta^{14}$C for (B) deep Atlantic (2,500m average depth), (C) abyssal Atlantic (3,700m average depth), (D) deep Pacific-Indian (2,500m average depth) and (E) abyssal Pacific-Indian (4,000m average depth). $\Delta\Delta^{14}$C is atmospheric minus ocean Δ^{14}C, to correct for the varying atmospheric Δ^{14}C signal. Model-data experiment results are shown as dots, with proxy data mean (solid lines) and one standard deviation (dashed lines) in each MIS. Model-data experiment results prior to MIS 4 are omitted, due to the radioactive decay of ^{14}C which precludes natural observations prior to ∼50 ka.

5 Discussion

5.1 Last glacial-interglacial cycle

This study applies a carbon cycle box model to diagnose the values for ocean circulation and Southern Ocean biological export productivity during the last glacial-interglacial cycle, optimised for ocean and atmospheric proxy data. This study continues efforts to simulate the last glacial-interglacial cycle of atmospheric CO_2 (e.g. Ganopolski et al., 2010; Brovkin et al., 2012; Menviel et al., 2012; Ganopolski and Brovkin, 2017), but with a simpler box model and using a non-transient model-data optimisation to estimate parameter values. There were three major episodes in which atmospheric CO_2 fell during the last

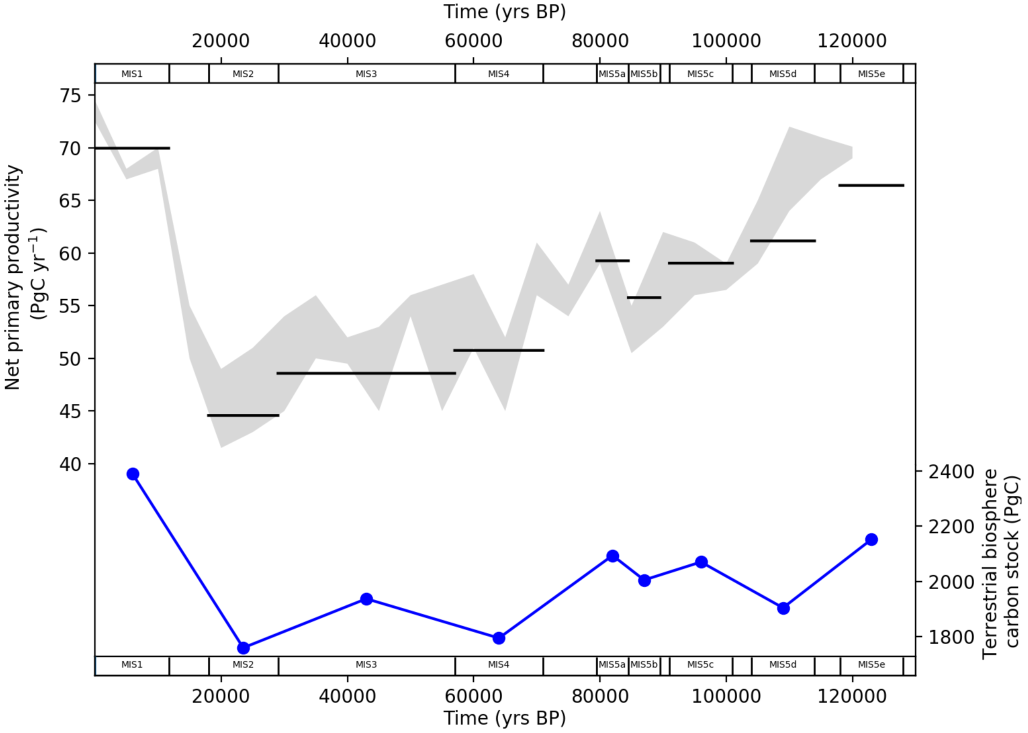

Figure 12. (A) Model-data output for the terrestrial biosphere net primary productivity (NPP) in each MIS time slice (black lines) compared with the range of estimates provided by Hoogakker et al. (2016) (grey area) and (B) model-data output for the terrestrial biosphere carbon stock for each MIS time slice.

glacial cycle (Fig. 4(A)). The first spanned 100-120 ka (MIS 5d-5e), which resulted in a decrease of ∼25 ppm. A second drop of ∼30ppm occurred during the period 60-80 ka (MIS 4-5a), and finally, a drop of ∼20 ppm took place more gradually during the period 20-40 ka in the lead up to the LGM (MIS 2-4). The cumulative effect of these discrete events, combined with other minor changes of ∼10 ppm throughout the glacial lead-up, was a drop in atmospheric CO_2 of ∼85 ppm below the penultimate interglacial period, ∼120-130 ka. Our model-data results show that atmospheric CO_2 and other proxy patterns are delivered by a host of physical and biogeochemical changes. These changes include weakened GOC, AMOC and strengthened Southern Ocean biological export productivity (Figs. 8,9,10,11), and changes in SST, salinity, ocean volume, the terrestrial biosphere, reef carbonates and atmospheric ^{14}C production (Fig. 2).

Our model-data results show that an initial fall in GOC took place at MIS 5d (Fig. 8), as atmospheric CO_2 fell by ∼30 ppm. This was also a time of substantial cooling in SST (Fig. 2(A)). GOC drifted lower until achieving its glacial minimum level in MIS 3 and MIS 2. A pronounced fall in AMOC took place at MIS 4, at the same time that North Atlantic SST cooled dramatically (Fig. 2(A)) and atmospheric CO_2 fell ∼30 ppm. GOC and AMOC were both equal to their glacial lows at the

LGM, and accompanied by increased Southern Ocean biological export productivity, yielding the LGM minima in atmospheric CO_2 and the final fall in CO_2 during the glacial cycle. We model elevated Southern Ocean biological productivity during MIS 2 and MIS 4, relative to interglacial values (MIS 1 and 5e). Importantly, the transition from MIS 3 to MIS 2, which incorporates the LGM and increased Southern Ocean biological productivity, only accounted for an average 13 ppm reduction in CO_2 (Figs. 4, 9). Therefore, our results suggest an increase in Southern Ocean biological productivity during this period was an additional 'kicker' to achieve the LGM CO_2 minima, following prior reductions of $\sim$70 ppm in the lead-up which were delivered mainly by ocean physical processes and SST. The finding of increased biological productivity, while mostly constrained to MIS 2-4, and a modest yet essential contributor to the overall glacial CO_2 drawdown, corroborates proxy data (e.g. Martinez-Garcia et al., 2014; Lambert et al., 2015; Kohfeld and Chase, 2017; Shaffer and Lambert, 2018) and recent model-data exercises (e.g. Menviel et al., 2016; Muglia et al., 2018). According to Shaffer and Lambert (2018), varying dust fertilisation of the surface ocean, and dust scattering effects on solar radiation, helped to push atmospheric CO_2 into and out of its glacial minima, for example at the LGM and last glacial termination.

For the Holocene, we model GOC and AMOC returning to values similar to the modern ocean estimates of Talley (2013). Our Holocene result for Atlantic (Pacific-Indian) Southern Ocean biological export productivity, of 3.8 (2.6) mol C m^{-2} yr^{-1} (Fig. 8), falls within modern observations for the Southern Ocean of 0.5-6 mol C m^{-2} yr^{-1} (e.g. Lourey and Trull, 2001; Weeding and Trull, 2004; Ebersbach et al., 2011; Jacquet et al., 2011; Cassar et al., 2015; Arteaga et al., 2019). Our model-data experiment results also reproduce values that fall within one standard deviation of the mean value in each model box, for all of the atmosphere and ocean proxies in each MIS (Figs. 9-11).

Kohfeld and Chase (2017) suggested that sequential falls in atmospheric CO_2 were first the result of temperature, sea-ice cover and potentially Atlantic Southern Ocean "barrier mechanisms" or shallow stratification, during MIS 5d-5e, and second, followed by falls in deep Atlantic ocean circulation and potentially dust-driven Southern Ocean biological productivity at MIS 4-5a. Finally, a synthesis of those factors with enhanced Southern Ocean biology, delivered the LGM CO_2 minimum. Our model-data results mostly agree with the Kohfeld and Chase (2017) hypothesis for glacial cycle CO_2, however we emphasise the role of ocean circulation in the Pacific and Indian oceans, in addition to the Atlantic Ocean. Stephens and Keeling (2000) proposed that expansive sea-ice cover around Antarctica, could deliver LGM CO_2 changes on its own as a result of reduced air-sea gas exchange, or in combination with ice-driven ocean stratification. However, Köhler et al. (2010) demonstrated with a carbon cycle box model that increased sea-ice cover leads to increased atmospheric CO_2, due to less in-gassing of CO_2 into the cold waters surrounding Antarctica. Kohfeld and Ridgewell (2009) reviewed estimates of the effects of *decreased* sea-ice cover at the last glacial termination and found a best estimate of -5 ppm within a range of -14-0 ppm, which is in the opposite direction to that envisaged by Stephens and Keeling (2000) and Kohfeld and Chase (2017). The modelling work by Stephens and Keeling (2000) was discounted by Kohfeld and Ridgewell (2009), because it assumed nearly all ocean-degassing of CO_2 was confined to the polar Antarctic region, when modern observations suggest the locus of outgassing is in the equatorial ocean (Takahashi et al., 2003). In SCP-M, the effects of polar Southern Ocean sea-ice cover, modelled as a slowing down in air-sea gas exchange in the polar surface box, are modest. This modelling result reflects the offsetting effects of upwelled nutrient- (and carbon) and rich waters (degassing and higher CO_2), against the effects of cooler temperatures and biological export productivity (in-gassing and lower CO_2). This finding may reflect our approach to treat polar sea-ice cover simply as a regulator of the rate of air-sea gas exchange in the polar oceans. This approach may neglect other effects of sea-ice cover including as a trigger for changes in Southern Ocean upwelling, NADW formation rates, deep ocean stratification, nutrient distributions and biological productivity (**?**Brovkin et al., 2012; Ferrari et al., 2014; Kohfeld and Chase, 2017; Jansen, 2017; Marzocchi and Jansen, 2017). For example, Brovkin et al. (2012) found that in the CLIMBER-2 model, atmospheric CO_2 was more sensitive to sea ice cover when it was linked to weakened vertical diffusivity in the Southern Ocean of tracers such as DIC, thereby reducing outgassing of CO_2.

In addition to cooling SST, increased-sea ice cover and other changes, SCP-M requires other changes in the ocean, to deliver the $\sim$25 ppm fall in CO_2 at MIS 5d-5e, and satisfy the other atmospheric and ocean proxy data. We model a weakening in GOC of $\sim$7 Sv at MIS 5d and further weakening until the LGM, a substantial change outside the Atlantic Basin and underscoring the importance of this feature in any hypothesis for the last glacial cycle or LGM-Holocene (Fig. 8). We note that our simplified representation of slowing GOC, as per Talley (2013), includes features that may be separated out or characterised differently in other models or hypotheses, such as AABW formation rate, Southern Ocean upwelling or shallow mixing/stratification, Pacific and Indian deepwater formation (PDW/IDW), or northward extension of AABW versus NADW formation of abyssal waters in the Atlantic Ocean (e.g. Menviel et al., 2016; Kohfeld and Chase, 2017).

The period MIS 5d-5e does not feature in many oceanographic theories of glacial inception, largely due to a focus on Atlantic ocean data and a lack of any obvious changes in the Atlantic shallow-deep-abyssal proxy offsets at that period, as observed clearly at MIS 4 and the LGM (e.g. Oliver et al., 2010; Yu et al., 2016; Kohfeld and Chase, 2017). However, Govin et al. (2009) proposed an expansion of AABW across the Southern Ocean at MIS 5d, and weakening of circumpolar deep water upwelling, based on qualitative analysis of deep ocean $\delta^{13}C$ from the Atlantic and Indian basins. The proxy evidence of Govin et al. (2009) supports the concept of De Boer and Hogg (2014), that the glacial ocean could have exhibited slower, and at the same time more expansive, formation of AABW. Ganopolski et al. (2010) and Brovkin et al. (2012) modelled cooling SST and substitution of North Atlantic Deep Water by denser waters of Antarctic origin, in the abyssal ocean, as the main drivers of falling atmospheric CO_2 at the last glacial inception. Menviel et al. (2012) modelled a transient slowdown in the rate of overturning circulation in the North Atlantic across MIS 5d-5e. Despite these findings, changes in ocean circulation at the last glacial inception are not obvious in Atlantic Ocean $\delta^{13}C$ proxy data (Oliver et al., 2010; Kohfeld and Chase, 2017).

To illustrate the plausibility of a slowdown in GOC at the last glacial inception, in the context of deep ocean $\delta^{13}C$ proxy data, we show a model experiment testing the sensitivity of atmospheric CO_2 and abyssal ocean $\delta^{13}C$ to slowed GOC under MIS 5d and MIS 5e conditions (Fig. 13). Shown for comparison are the standard deviation of data values for abyssal ocean $\delta^{13}C$ for MIS 5e (Fig. 13(B)). The experiment shows that slowing GOC from the MIS 5e model-data optimised value of 29 Sv (e.g. Fig. 8), delivers lower values for CO_2 (Fig. 13A) and more negative abyssal Pacific-Indian $\delta^{13}C$ (Fig. 13B). However, in the experiment of decreasing GOC, modelled Atmospheric CO_2 crosses the $\sim$25 ppm change of the MIS 5d-5e transition, well before the model's abyssal Pacific-Indian box $\delta^{13}C$ breaches one standard deviation of the abyssal Pacific-Indian $\delta^{13}C$ data (Fig. 13(B)). Changes in the deep-abyssal $\delta^{13}C$ offsets are also muted (Figure 13(C)) relative to atmospheric CO_2, and particularly for the Atlantic Ocean. The observation is even more obvious when including other ocean changes for the MIS

5d-5e transition, such as SST, in the experiment. When these changes are incorporated (shown as the "x" symbols in Fig. 13(A and B), the atmospheric CO_2 change across MIS 5d-5e is even more quickly satisfied by the modelled reduction in GOC, while abyssal ocean δ^{13}C remains near its MIS 5d box average, and well within one standard deviation. Despite a range of GOC variation that surpasses the MIS 5d-5e CO_2 reduction, the abyssal Atlantic δ^{13}C result hardly varies, a particularly interesting finding. In SCP-M this can be explained by a reduced rate of AABW formation as a part of slowing GOC, leading to relatively greater influence of other Atlantic Ocean processes, such as the deep-abyssal mixing and AMOC, which mixes deep water with a more positive δ^{13}C into the abyssal Atlantic and offsets the effects of slowing GOC. Slowing GOC by itself leads to a more negative abyssal δ^{13}C, as per the Pacific-Indian Basin results. This type of dynamic could help explain why hypothesised or modelled changes in the ocean at the last glacial inception (e.g. Govin et al., 2009; Menviel et al., 2012; Brovkin et al., 2012) don't show up more obviously in the deep and abyssal Atlantic Ocean δ^{13}C proxy data (Oliver et al., 2010; Kohfeld and Chase, 2017).

These observations from Fig. 13 could be exaggerated in SCP-M due to the large size of its ocean boxes and therefore relatively large spread of δ^{13}C values and standard deviations for each box. In addition, this experiment may reflect idiosyncrasies in the SCP-M model design and its simple parameterisation of ocean circulation and mixing. A finer resolution model may show a greater sensitivity of the ocean box δ^{13}C to variations in ocean circulation. Menviel et al. (2015) analysed the sensitivity of ocean and atmospheric δ^{13}C to variations in NADW, AABW and North Pacific Deep Water (NPDW) formation rates, in the context of rapid changes in atmospheric δ^{13}C and CO_2 observed during the last glacial termination. Their modelling, using the more spatially-detailed LOVECLIM and Bern3D models, showed modest but location-dependent sensitivities of ocean δ^{13}C to slowing ocean circulation, and particular sensitivity to AABW. These models are much higher resolution and show greater sensitivity of δ^{13}C to ocean circulation over depth intervals not differentiated in the SCP-M boxes, but also quite a variation across the LOVECLIM and Bern3D models. However, our simple experiment illustrated in Fig. 13 does highlight the potential for important changes in the ocean during glacial-interglacial periods to go unnoticed, when focussed on one set of ocean proxy data and without validation by modelling.

As shown in Fig. 13, analysing Atlantic Ocean data in isolation, and only qualitatively assessing ocean proxy data offsets (e.g. solely relying on standard deviations), may obscure features that could have contributed meaningfully to glacial falls in atmospheric CO_2 (e.g. GOC). According to (Talley, 2013) GOC is a key part of the global ocean carbon cycle, operating in the Atlantic, Pacific and Indian ocean basins. Given it's a global feature, spread across all basins, its global changes may not show up as dramatic changes in proxy data offsets in any particular basin, despite it exerting a strong influence on atmospheric CO_2. A number of authors highlight changes in Δ^{14}C distributions in the Pacific Ocean during the LGM and Holocene, providing qualitative evidence of changes in ocean circulation in this basin and of it being a potential driver for post-glacial increase in atmospheric CO_2 (e.g. Sikes et al., 2000; Marchitto et al., 2007; Stott et al., 2009; Cook and Keigwin, 2015; Skinner et al., 2015; Ronge et al., 2016; Skinner et al., 2017). Ocean Δ^{14}C values are particularly sensitive to ocean circulation rates (Broecker et al., 1980). However, Δ^{14}C proxy records in periods prior to the LGM and Holocene are sparse, because they can only extend to $\sim$50 ka due to their radioactive decay in nature, therefore cannot be applied to the glacial inception period.

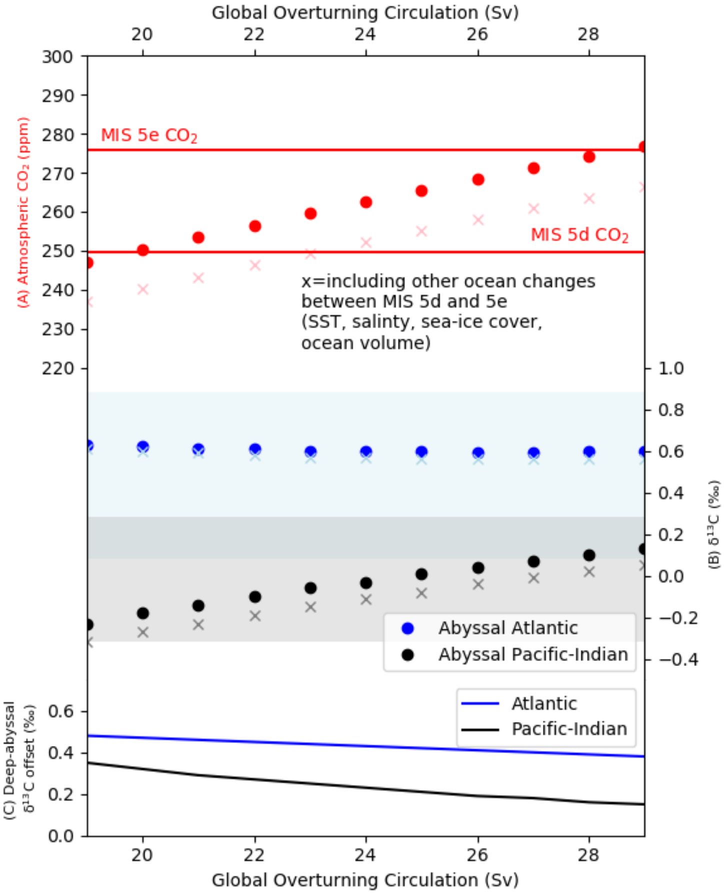

Figure 13. Sensitivity of atmospheric CO_2 and ocean $\delta^{13}C$ to a downward variation in global ocean circulation parameter Ψ_1 in MIS 5e in SCP-M. x-axis shows the range of variation in Ψ_1 in Sv and the y-axes show the model results for (A) atmospheric CO_2 and (B) abyssal ocean $\delta^{13}C$ in each basin. Shaded areas are the ± standard deviations for abyssal $\delta^{13}C$ in MIS 5e. (C) shows the deep-abyssal $\delta^{13}C$ offset for each basin. Atmospheric CO_2 in MIS 5d and 5e is shown for reference. The "x" symbols in (A) and (B) show the same experiment including other changes in the ocean across MIS 5d-5e: SST, salinity, sea-ice cover, ocean volume and coral reef carbonate production. Southern Ocean biological export productivity is not varied in this experiment.

There is qualitative multi-proxy evidence for a slowdown or shoaling of AMOC at MIS 4. Kohfeld and Chase (2017) evaluated Atlantic basin $\delta^{13}C$ data and surmised that Atlantic deep ocean circulation slowed or shoaled at MIS 4. Yu et al. (2016) and Chalk et al. (2019) came to similar conclusions from analysis of carbonate proxy records. Piotrowski et al. (2009) further suggested a reduced proportion of AMOC-sourced waters in the deep Indian Ocean at MIS 4, as deduced from Indian Ocean $\delta^{13}C$ data. Our model-data results corroborate these findings, with a pronounced weakening in AMOC at MIS 4. SCP-M does not take explicit account of AMOC shoaling due to it’s rigid box boundaries, and therefore the change in proxy data across MIS 4-5a is resolved as weakening AMOC, which could understate the importance of this event. We also model a drop in AMOC at MIS 5b which replicates abyssal Atlantic δ^{13}C and CO_3^{2-}observations (Fig. 5 and Fig. 7), and also accompanies a transient fall in atmospheric CO_2 of 14 ppm at that period (Fig. 4). Menviel et al. (2012) modelled a transient, but more dramatic decline in the rate of overturning circulation in the Atlantic Ocean at MIS 5b, and a more protracted but similarly large decline during MIS 4 (also modelled by Ganopolski et al. (2010)), in addition to a deepening in the remineralisation depth of organic carbon.

Our model-data results indicate a role for increased Southern Ocean biological export productivity in achieving glacial troughs in atmospheric CO_2 in MIS 4 and MIS 2. Our finding of increased biological productivity, while mostly constrained to MIS 2 and MIS 4, and a modest contributor to the overall glacial CO_2 drawdown, aligns with proxy data for increased iron-rich continental dust supply to the Southern Ocean in these periods (e.g. Martinez-Garcia et al., 2014; Lambert et al., 2015; Kohfeld and Chase, 2017) and recent model-data exercises (e.g. Menviel et al., 2016; Muglia et al., 2018; Khatiwala et al., 2019). Martin (1990) pioneered the "iron hypothesis", which invoked the increased supply of continent-borne dusts to the Southern Ocean in glacial periods. Increased dust supply stimulated more plankton productivity where plankton were bio-limited in nutrients supplied in the dust, such as iron (Martin, 1990). Since then, the iron hypothesis has retained an important place in the debate over glacial-interglacial cycles of CO_2. Watson et al. (2000) took experimental data on the effects of iron supply on plankton productivity in the Southern Ocean (Boyd, 2000) and applied this to a carbon cycle model across glacial-interglacial cycles. Their modelling, informed by the ocean experiment data, suggested that variations in the Southern Ocean iron supply and plankton productivity could account for large ($\sim$40 ppm) swings in atmospheric CO_2, with peak activity in the last glacial cycle at MIS 2 and MIS 4. Debate has continued over the magnitude of the contribution of Southern Ocean biological productivity to the glacial CO_2 drawdown. According to Kohfeld et al. (2005), based on sediment data, the Southern Ocean biological productivity mechanism could account for no more than half of the glacial CO_2 drawdown. Others emphasise that Southern Ocean biological export productivity fluxes may have been weaker in the LGM, in absolute terms, but that with weaker Southern Ocean upwelling, the iron-enhanced productivity contributed to a stronger biological pump of carbon and was a major contributor to the LGM CO_2 drawdown (Jaccard et al., 2013; Martinez-Garcia et al., 2014; Yamamoto et al., 2019).

Figure 14 shows the contribution to the glacial drawdown in atmospheric CO_2 by each mechanism we modelled, relative to the penultimate interglacial period (MIS 5e), in SCP-M. Our model-data study finds that approximately half of the glacial atmospheric CO_2 drawdown is contributed by weakened ocean circulation (GOC and AMOC), with the other half contributed by a combination of cooler SST, increased Southern Ocean biological export productivity, varying coral reef carbonate production and dissolution, and increased sea-ice cover. Weakened GOC delivers the highest contribution to falling CO_2, followed by cooler SST, weakened AMOC and stronger Southern Ocean biological export productivity. Lower SST leads to modest reductions in CO_2 early in the glacial cycle, increasing as the ocean cools further in MIS 4, and is an important contributor to decreased CO_2 in the LGM (Kohfeld and Chase, 2017). Southern Ocean biological export productivity strengthens at MIS 4, and contributes a peak of -10 ppm by MIS 2 (LGM). Other parameters contribute minor increases in CO_2 (salinity, polar sea-ice, ocean volume) and decreases (coral reefs) during the cycle. Our estimate for coral reefs, of -8 ppm CO_2, is at the lower end of the range of 6-20 ppm summarised in Kohfeld and Ridgewell (2009), suggesting that our simple parameterisation of the coral reef carbon and alkalinity fluxes could underestimate its effect, likely due to the assumed fast mixing rates of reef carbon and alkalinity into the surface boxes in SCP-M. Ridgwell et al. (2003) modelled +20 ppm CO_2 from coral reef accumulation in the Holocene period, noting a high sensitivity of their model to coral reef accumulation rates. These attributions in Fig. 14 include the effects of feedbacks in the carbon cycle, such as carbonate compensation in the ocean, and the terrestrial biosphere - which responds to declining atmospheric CO_2. The terrestrial biosphere is discussed in more detail below. It is likely that our model-data results underestimate the contribution of AMOC, which is hypothesised to slow and/or shoal during the period MIS 2-4 (e.g. Menviel et al., 2012; Brovkin et al., 2012; Yu et al., 2016; Eggleston et al., 2016; Kohfeld and Chase, 2017). Our model does not explicitly resolve shoaling, other than a linear-positive linkage between the AMOC circulation parameter and a deep-abyssal Atlantic box mixing term (less mixing between the deep and abyssal Atlantic boxes as AMOC slows), and therefore may serve to miss additional parts of the AMOC mechanism which could contribute to greater atmospheric CO_2 drawdown in Fig. 14. The contribution of the model parameters to the glacial atmospheric CO_2 drawdown shown in Fig. 14, incorporate the effects of various feedbacks in the model such as the terrestrial biosphere, continental weathering, and calcium carbonate compensation. Shown for comparison on the right axis of Fig. 14 is the impact on atmospheric CO_2 from the contraction of the terrestrial biosphere through the glacial cycle from MIS 5e. The effects are similar yet modestly higher than Ganopolski and Brovkin (2017), reflecting the larger change in the terrestrial biosphere carbon stock in the lead up to the LGM from MIS 5e, from this study (-400 Pg C (and ∼+630 Pg C from MIS 2 to MIS 1)), compared with the glacial-interglacial estimate of Ganopolski and Brovkin (2017) (-350 Pg C).

5.2 The LGM and Holocene

Within the context of LGM-Holocene studies, our findings corroborate the hypothesis that a number of mechanisms, not one singular factor, delivered the ∼85 ppm increase in atmospheric CO_2 from the LGM to the Holocene (e.g. Kohfeld and Ridgewell, 2009; Sigman et al., 2010; Hain et al., 2010; Menviel et al., 2012; Brovkin et al., 2012; Ferrari et al., 2014; Menviel et al., 2016; Ganopolski and Brovkin, 2017; Kohfeld and Chase, 2017; Muglia et al., 2018). This finding is more obvious when the sequential nature of changes is observed over the full glacial cycle, as distinct from analysing the LGM and Holocene in isolation. Our model-data results agree with those of Menviel et al. (2016): that variations primarily in GOC and AMOC, SST, and alongside Southern Ocean biological productivity, can account for for atmospheric CO_2 variation from the LGM to the Holocene, with an opposing feedback provided by the terrestrial biosphere. The longer time timescale of our analysis highlights that changes in GOC and AMOC took place much earlier in the glacial cycle than the LGM, and were at or near their glacial minima prior to the LGM. Our model-data results also constrain the effects of Southern Ocean biological export productivity in the glacial cycle CO_2, to MIS 2-4. Enhanced wind-borne iron dust deposits over the Southern Ocean are believed to have fed increased phytoplankton growth in the LGM and possibly MIS 4 (Martin, 1990; Martinez-Garcia et al., 2014; Kohfeld and Chase, 2017; Muglia et al., 2018).

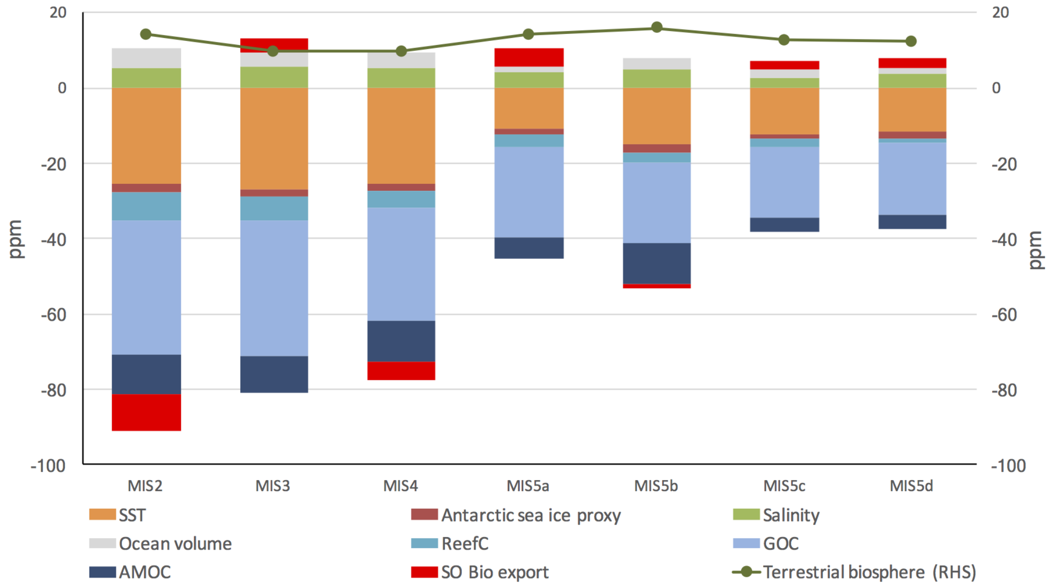

Figure 14. Impacts on CO_2 of model parameters from the model-data experiment results, from the penultimate interglacial period (MIS 5e) to the Last Glacial Maximum (MIS 2). SST = sea surface temperature, ReefC = shallow carbonate production/dissolution, GOC = global ocean circulation, AMOC = Atlantic Meridional Overturning Circulation, SO Bio Export = Southern Ocean Biological export productivity. Shown for comparison is the impact of the terrestrial biosphere in each MIS stage (comparison between model runs with and without terrestrial biosphere).

5.3 The terrestrial biosphere

Our modelled increase in the terrestrial biosphere carbon stock from the LGM to Holocene, of ∼630 Pg C (Fig. 12), falls within, but towards the upper end of, recent estimates of this change, of 300-850 Pg C (e.g. Joos et al., 2004; Brovkin et al., 2007; Köhler et al., 2010; Prentice et al., 2011; Brovkin et al., 2012; Ciais et al., 2012; Peterson et al., 2014; Menviel et al., 2016; Jeltsch-Thommes et al., 2019)). For example, Peterson et al. (2014) estimated a variation of 511 ± 289 Pg C in the terrestrial biosphere carbon stock, based on whole of ocean δ^{13}C data. Brovkin et al. (2007), Brovkin et al. (2012) and Köhler et al. (2010) all modelled ∼500-550 Pg C increase in the terrestrial biosphere between the LGM and Holocene (Prentice et al. (2011) estimated (550-694 Pg C)). According to Francois et al. (1999), palynological and sediment data infer that the terrestrial biosphere carbon stock was 700-1350 Pg C smaller in the LGM than the present. Ciais et al. (2012) pointed to a growth of a large carbon pool in steppes and tundra during the LGM as an offsetting feature to the declining tropical biosphere, a feature also included in reconstructed last glacial terrestrial biosphere by Hoogakker et al. (2016), leading to a smaller estimate of ∼330 Pg C (Ganopolski and Brovkin (2017) modelled a similar estimate of 350 Pg C). Jeltsch-Thommes et al. (2019) estimated a glacial-interglacial change in terrestrial biosphere of 850 Pg C (median estimate; range 450 to 1250 Pg C), a similar estimate to that of Joos et al. (2004) of 820-850 Pg C. Jeltsch-Thommes et al. (2019) demonstrated the importance of including ocean-sediment and weathering fluxes in their modelling estimates, and suggested other studies may underestimate the full deglacial change in the terrestrial biosphere carbon stock. While our model results (∼630 Pg C) are higher than some estimates of the LGM-Holocene change in the terrestrial biosphere (e.g. Ciais et al., 2012; Menviel et al., 2016; Ganopolski and Brovkin, 2017), they are mostly in good agreement (e.g. Joos et al., 2004; Brovkin et al., 2007; Köhler et al., 2010; Prentice et al., 2011; Brovkin et al., 2012; Peterson et al., 2014; Jeltsch-Thommes et al., 2019), and our NPP estimates mostly align with the glacial cycle NPP reconstruction of Hoogakker et al. (2016) as shown in Fig. 12. The driver for NPP in the simple terrestrial biosphere module in SCP-M is atmospheric CO_2, via carbon fertilisation. According to several authors (e.g. Otto et al., 2002; Kaplan et al., 2002; Joos et al., 2004; Hoogakker et al., 2016), carbon fertilisation is the primary driver of global variation in the terrestrial biosphere NPP during the last glacial-interglacial cycle. However, the importance of carbon fertilisation versus temperature and precipitation, and other factors, as drivers of NPP, are debated (e.g. Francois et al., 1999; van der Sleen et al., 2015).

5.4 Advantages and limitations of this study

The use of a simple box model for this model-data study, SCP-M, enabled a range of proxies to be incorporated into the MIS reconstructions, and a large number of simulations (∼9,000) to explore possible parameter combinations in each MIS. However, given the large spatial coverage of the SCP-M boxes, data for large areas of the ocean are averaged, and some detail is lost. For example, in the case of the carbonate ion proxy, we apply a default estimate of standard deviation to account for the large volume of ocean covered by SCP-M's boxes relative to the proxy data locations, and to enable the normalisation of the carbonate ion proxy data in a procedure that uses the data standard deviation as a weighting. Despite this caveat, we believe that the model-data experiment results provide a good match to the data across the various atmospheric and ocean proxies as shown in Figs 9-11.

Most major processes in the SCP-M model are simply parameterised, allowing them to be free-floated in model-data experiments. However, the driving factors behind parameter value changes can only be speculated. For example, slowdown in GOC may be the result of changing wind patterns or buoyancy fluxes around Antarctica (Morrison and Hogg, 2013), Antarctic sea-ice cover (Ferrari et al., 2014), or may be the result of shoaling AMOC leading to extensive filling of the abyssal ocean by waters sourced from GOC (Curry and Oppo, 2005; De Boer and Hogg, 2014; Jansen, 2017). Probing the root cause of our model-data findings would require a more detailed physical and/or biogeochemical model. Furthermore, we apply a simple representation of the terrestrial biosphere in our model-data experiments, relying primarily on atmospheric CO_2 as the driver for NPP. This approach provided reasonable results for the terrestrial biosphere carbon stock and NPP, on the whole, but may miss some detail in the terrestrial biosphere during the last glacial-interglacial cycle. Our MIS time-slicing obscures details in the proxy records within MIS. For example, Yu et al. (2013) observed a transient drop in carbonate ion concentrations in the deep Pacific Ocean during MIS 4, and there are large transient changes in atmospheric $\delta^{13}C$ during MIS 3-4. Ganopolski et al. (2010) and Menviel et al. (2012) modelled transient collapses and rebounds in AMOC during MIS 4 (and other short-term changes in atmospheric dust supply and depth of biological nutrient remineralisation), which could have contributed to the full observed magnitude of changes in atmospheric $\delta^{13}C$ across this period (e.g. Eggleston et al., 2016) - not captured with our

MIS-averaging approach. We omitted the transient last glacial termination from our analysis, a period in which atmospheric CO_2 rose $\sim$85 ppm in 8 kyr. Future model-data optimisation work could probe this period at 1 kyr intervals, or with transient, data-optimised simulations, to profile the unwinding of processes that led to the last glacial cycle CO_2 drawdown. In summary, while the model we applied is high level in nature, the modelling itself is heavily constrained by natural observations and proxy data from the carbon cycle. Therefore, this work presents a plausible set of modelled outcomes for the last glacial-interglacial cycle.

6 Conclusions

Multiple processes drove atmospheric CO_2 fluctuations during the last glacial cycle. Against a backdrop of varied SST, salinity, sea-ice cover, ocean volume and reef carbonates, we modelled sequentially weaker GOC (first) and AMOC (second) to reduce atmospheric CO_2 in the lead up to the LGM. At the LGM, increased Southern Ocean biological export productivity delivered an incremental fall in CO_2, resulting in the glacial cycle CO_2 minimum. GOC, AMOC, Southern Ocean biology and SST rebounded to modern values between the LGM and Holocene, contributing to the sharp post-glacial increase in CO_2. The terrestrial biosphere played an important negative feedback role during the glacial cycle, releasing δ^{13}C-negative CO_2 to the atmosphere at times during the glaciation, and taking up CO_2 during the termination and Holocene. These model-data results were achieved with a simple carbon cycle box optimised for proxy data for CO_2, δ^{13}C, Δ^{14}C and $CO^{2-}{}_3$. Our results agree with hypotheses for glacial-interglacial cycle CO_2 that emphasise varying ocean circulation, include marine biological productivity, and amidst many other physical and biogeochemical changes in the marine and terrestrial carbon cycle (e.g. Kohfeld and Ridgewell, 2009; Sigman et al., 2010; Ganopolski et al., 2010; Brovkin et al., 2012; Menviel et al., 2012; Ferrari et al., 2014; Menviel et al., 2016; Kohfeld and Chase, 2017; Ganopolski and Brovkin, 2017). We emphasise the need to include the Pacific and Indian oceans in evaluation of the oceanic carbon cycle, particularly in relation to the last glacial cycle and the LGM-Holocene transition.

Many uncertainties exist in the data and the prescribed nature of the processes in a box model. However, such uncertainty is largely inescapable when dealing with models and proxy data. We propose these model-data results as one set of plausible results for the last glacial carbon cycle, in agreement with available proxy data, and see them as encouraging for the use of models and data to help constrain hypotheses for the paleo- carbon cycle.

7 Code and data availability

The model code, processed data files, model-data experiment results, and any (published) raw proxy data gathered in the course of this work, are located at https://doi.org/10.5281/zenodo.3559339. No original data was created, or unpublished data used, in this work. This paper's Supplementary Information contains an overview of the files contained in the repository. For more detail on the SCP-M equations, see O'Neill et al. (2019).

Author contributions. CO undertook model development work, data-gathering, modelling and model-data experiments. AH provided the oceanographic interpretation and guided modelling and data analysis. ME designed model-data experiments and provided input into data analysis and the modelling of the marine biology and isotopes. BO contributed glacial cycle model forcings and input to modelling of the reef carbonates. SE oversaw the modelling of the marine biology and carbonate pump. All authors contributed to drafting and reviewing the document.

Competing interests. The authors declare that they have no conflict of interest.

Acknowledgements. Stewart Fallon provided input to the processing of radiocarbon data. Malcolm Sambridge provided input on model-data optimisation and inversions. Jimin Yu provided helpful discussions and carbonate ion proxy data.

References

Adkins, J., McIntyre, K., and Schrag, D.: The Salinity, Temperature, and 18O of the Glacial Deep Ocean, Science, 298, 1769–1773, 2002.

Anderson, R., Chase, Z., Fleisher, M., and Sachs, J.: The Southern Ocean's biological pump during the Last Glacial Maximum, Deep Sea Research Part II: Topical Studies in Oceanography, 49, 1909–1938, 2002.

Archer, D. and Maier-Reimer, E.: Effect of deep-sea sedimentary calcite preservation on atmospheric CO2 concentration, Nature, 367, 260–263, 1994.

Arneth, A., Sitch, S., and J. Pongratz, e. a.: Historical carbon dioxide emissions caused by land-use changes are possibly larger than assumed, Nature Geoscience, 10,, 79–84, 2017.

Arteaga, L., Pahlow, M., Bushinsky, S., and Sarmiento, J.: Nutrient Controls on Export Production in the Southern Ocean, Global Biogeochemical Cycles, 33, 942–956, 2019.

Barker, S., Knorr, G., Vautravers, M., Diz, P., and Skinner, L.: Extreme deepening of the Atlantic overturning circulation during deglaciation, Nature Geoscience, 3, 567–571, 2010.

Bereiter, B., Eggleston, S., Schmitt, J., Nehrbass-Ahles, C., Stocker, T., Fischer, H., Kipfstuhl, S., and Chappellaz, J.: Revision of the EPICA Dome C CO2 record from 800 to 600kyr before present, Geophys. Res. Lett, 2015.

Berger, W.: Increase of carbon dioxide in the atmosphere during deglaciation: The coral reef hypothesis, Naturwissenschaften, 69, 87–88, 1982.

Boyd, P. e. a.: A mesoscale phytoplankton bloom in the polar Southern Ocean stimulated by iron fertilization, Nature, pp. 695–702, 2000.

Broecker, W., Yu, J., and Putnam, A.: Two contributors to the glacial CO2 decline, Earth and Planetary Science Letters, pp. 191–196, 2015.

Broecker, W. S.: Ocean chemistry during glacial time, Geochim. Cosmochim. Acta, 46, 1689–1705, 1982.

Broecker, W. S. and Barker, S.: A 190‰ drop in atmosphere's Δ14C during the "Mystery Interval" (17.5 to 14.5 kyr), Earth and Planetary Science Letters, 256, 90–99, 2007.

Broecker, W. S., Peng, T. H., and Engh, R.: Modeling the carbon system, Radiocarbon, 22, 565–598, 1980.

Brovkin, V., Claussen, J. B. M., Ganopolski, A., Kubatzki, C., Petoukhov, V., and Andreev, A.: Carbon cycle, vegetation, and climate dynamics in the Holocene: Experiments with the CLIMBER-2 model, Global Biogeochemical Cycles, 16, 1139, doi:10.1029/2001GB001 662, 2002.

Brovkin, V., Ganopolski, A., Archer, D., and Rahmstorf, S.: Lowering of glacial atmospheric CO2 in response to changes in oceanic circulation and marine biogeochemistry, Paleoceanography, 22, PA4202, doi:10.1029/2006PA001 380, 2007.

Brovkin, V., Ganopolski, A., Archer, D., and Munhoven, G.: Glacial CO2 cycle as a succession of key physical and biogeochemical processes, Climate of the Past, 8, 251–264, 2012.

Bryan, S., Marchitto, T., and Lehman, S.: The release of 14C-depleted carbon from the deep ocean during the last deglaciation: Evidence from the Arabian Sea, Earth and Planetary Science Letters, 298, 244–254, 2010.

Burke, A. and Robinson, L.: The Southern Ocean's Role in Carbon Exchange During the Last Deglaciation, Science, 335, 557–561, 2012.

Cassar, N., Wright, S., Thomson, P., Trull, T., Westwood, K., de Salas, M., Davidson, A., Pearce, I., Davies, D., and Matear, R.: The relation of mixed-layer carbon export production to plankton community in the Southern Ocean, Global Biogeochemical Cycles, 29, 446–462, 2015.

Chalk, T., Foster, G., and Wilson, P.: Dynamic storage of glacial CO2 in the Atlantic Ocean revealed by boron [CO2-3] and pH records, Earth and Planetary Science Letters, 510, 1–11, 2019.

Chen, T., Robinson, L., Burke, A., Southon, J., Spooner, P., Morris, P., and Ng, H.: Synchronous centennial abrupt events in the ocean and atmosphere during the last deglaciation, Science, 349, 1537–1541, 2015.

Ciais, P., Tagliabue, A., Cuntz, M., Bopp, L., Scholze, M., Hoffmann, G., Lourantou, A., Harrison, S. P., Prentice, I. C., Kelley, D. I., Koven, C., and Piao, S. L.: Large inert carbon pool in the terrestrial biosphere during the Last Glacial Maximum, Nature Geoscience, 5, 74–79, 2012.

Collatz, G., Berry, J., and Clark, J.: Effects of climate and atmospheric CO2 partial pressure on the global distribution of C4 grasses: present, past, and future, Oecologia, 114, 441–454, 1998.

Cook, M. and Keigwin, L.: Radiocarbon profiles of the NW Pacific from the LGM and deglaciation: Evaluating ventilation metrics and the effect of uncertain surface reservoir ages, Paleoceanography, pp. 174–195, 2015.

Curry, W. B. and Oppo, D. W.: Glacial water mass geometry and the distribution of d13C of CO2 in the western Atlantic Ocean, Paleoceanography, 20, PA1017, doi:10.1029/2004PA001 021, 2005.

Davies-Walczak, M., Mix, A., Stoner, J., Southon, J., Cheseby, M., and Xuan, C.: Late Glacial to Holocene radiocarbon constraints on North Pacific Intermediate Water ventilation and deglacial atmospheric CO2 sources, Earth and Planetary Science Letters, 397, 57–66, 2014.

De Boer, A. M. and Hogg, A. M. C.: Control of the glacial carbon budget by topographically induced mixing, Geophys. Res. Lett, 41, 4277–4284, 2014.

DeVries, T. and Weber, T.: The export and fate of organic matter in the ocean: New constraints from combining satellite and oceanographic tracer observations, Paleoceanography, 31, 535–555, 2017.

Dunne, J. P., Armstrong, R. A., Gnanadesikan, A., and Sarmiento, J. L.: Empirical and mechanistic models for the particle export ratio, Global Biogeochemical Cycles, 19, GB4026, doi:10.1029/2004GB002 390, 2005.

Ebersbach, F., Trull, W., Davies, D., and Bray, S.: Controls on mesopelagic particle fluxes in the Sub-Antarctic and Polar Frontal Zones in the Southern Ocean south of Australia in summer - Perspectives from free-drifting sediment traps, Deep Sea Research Part II: Topical Studies in Oceanography, 58, 2260–2276, 2011.

Eggleston, S., Schmitt, J., Bereiter, B., Schneider, R., and Fischer, H.: Evolution of the stable carbon isotope composition of atmospheric CO2 over the last glacial cycle, Paleoceanography, 31, 434–452, 2016.

Ferrari, R., Jansen, M., Adkins, J., Burke, A., Stewart, A. L., and Thompson, A.: Antarctic sea ice control on ocean circulation in present and glacial climates, PNAS, 111, 8753–8758, 2014.

Follows, M. J., Ito, T., and Dutkiewicz, S.: On the solution of the carbonate chemistry system in ocean biogeochemistry models, Ocean Modelling, 12, 290–30, 2006.

Francois, L., Godderis, Y., Warnant, P., Ramstein, G., de Noblet, N., and Lorenz, S.: Carbon stocks and isotopic budgets of the terrestrial biosphere at mid-Holocene and last glacial maximum times, Chemical Geology, 159, 163–199, 1999.

Freeman, E., Skinner, L., Waelbroeck, C., and Hodell, D.: Radiocarbon evidence for enhanced respired carbon storage in the Atlantic at the Last Glacial Maximum, Nature Communications, 2016.

Ganopolski, A. and Brovkin, V.: Simulation of climate, ice sheets and CO2 evolution during the last four glacial cycles with an Earth system model of intermediate complexity, Climate of the Past, 13, 1695–1716, 2017.

Ganopolski, A., Calov, R., and Claussen, M.: Simulation of the last glacial cycle with a coupled climate ice-sheet model of intermediate complexity, Climate of the Past, 6, 229–244, 2010.

Govin, A., Michel, E., Labeyrie, L., Waelbroeck, C., Dewilde, F., and Jansen, E.: Evidence for northward expansion of Antarctic Bottom Water mass in the Southern Ocean during the last glacial inception, Paleoceanography, 24, doi:10.1029/2008PA001 603, 2009.

Hain, M. P., Sigman, D. M., and Haug, G. H.: Carbon dioxide effects of Antarctic stratification, North Atlantic Intermediate Water formation, and subantarctic nutrient drawdown during the last ice age: Diagnosis and synthesis in a geochemical box model, Global Biogeochem. Cycles, 24, GB4023, doi:10.1029/2010GB003 790, 2010.

Harman, I., Trudinger, C., and Raupach, M.: SCCM – the Simple Carbon-Climate Model: Technical Documentation, CAWCR Technical Report 047, CSIRO Centre for Australian Weather and Climate Research, CSIRO Marine and Atmospheric Research, FC Pye Laboratory, GPO Box 3023, Canberra, ACT, 2601, Australia, 2011.

Harrison, K. G.: Role of increased marine silica input on paleo-pCO2 levels, Paleoceanography, 15, 292–298, 2000.

Henson, S. A., Sanders, R., Madsen, E., Morris, P. J., Moigne, F. L., and Quartly, G. D.: A reduced estimate of the strength of the ocean's biological carbon pump, Geophys. Res. Lett., 38, L04 606, doi:10.1029/2011GL046 735, 2011.

Hines, S., Southon, J., and Adkins, J.: A high-resolution record of Southern Ocean intermediate water radiocarbon over the past 30,000 years, Earth and Planetary Science Letters, 432, 46–48, 2015.

Hoff, U., Rasmussen, T., Stein, R., Ezat, M., and Fahl, K.: Sea ice and millennial-scale climate variability in the Nordic seas 90 kyr ago to present, Nature Communications, 7, DOI: 10.1038/ncomms12 247, 2015.

Hogg, A. M.: Glacial cycles and carbon dioxide: A conceptual model, Geophys. Res. Lett., 35, L01 701, doi:10.1029/2007GL032 071, 2008.

Hoogakker, B. et al.: Terrestrial biosphere changes over the last 120 kyr, Climate of the Past, 12, 51–73, 2016.

Huang, Y., Street-Perrott, F., Metcalfe, S., Brenner, M., Moreland, M., and Freeman, K.: Climate change as the dominant control on glacial-interglacial variations in C3 and C4 plant abundance, Science, 293, 1647–1651, 2001.

Jaccard, S., Hayes, C., Martínez-García, A., an R.F. Anderson, D. H., Sigman, D., and Haug, G.: Two Modes of Change in Southern Ocean Productivity Over the Past Million Years, Science, 339, 1419–1423, 2013.

Jacquet, S., Lam, P., Trull, T., and Dehairs, F.: Carbon export production in the Polar Front Zone and Subantarctic Zone south of Tasmania, Deep Sea Research Part II: Topical Studies in Oceanography, 58, 2277–2292, 2011.

Jansen, M.: Glacial ocean circulation and stratification explained by reduced atmospheric temperature, PNAS, 114, 45–50, 2017.

Jeltsch-Thommes, A., Battaglia, G., Cartapanis, O., Jaccard, S., and Joos, F. J.: Low terrestrial carbon storage at the Last Glacial Maximum: constraints from multi-proxy data, Climate of the Past, 15, 849–879, 2019.

Joos, F., Gerber, S., Prentice, I. C., Otto-Bliesner, B., and Valdes, P.: Transient simulations of Holocene atmospheric carbon dioxide and terrestrial carbon since the Last Glacial Maximum, Global Biogeochemical Cycles, 18, GB2002, doi:10.1029/2003GB002 156, 2004.

Kaplan, J., Prentice, I., Knorr, W., and Valdes, P.: Modeling the dynamics of terrestrial carbon storage since the Last Glacial Maximum, Geophysical Research Letters, 22, 2074, doi:10.1029/2002GL015 230, 2002.

Key, R.: Ocean process tracers: Radiocarbon. In: Encyclopedia of Ocean Sciences, pp. 2338–2353, Academic Press, London, 2001.

Key, R., Kozyr, A., Sabine, C. L., Lee, K., Wanninkhof, R., Bullister, J. L., Feely, R. A., Millero, F. J., Mordy, C., and Peng, T.-H.: A global ocean carbon climatology: Results from Global Data Analysis Project (GLODAP), Global Biogeochemical Cycles, 18, GB4031, doi:10.1029/2004GB002 247, 2004.

Khatiwala, S., Schmittner, A., and Muglia, J.: Air-sea disequilibrium enhances ocean carbon storage during glacial periods, Science Advances, 5, doi:10.1126/sciadv.aaw4981, https://advances.sciencemag.org/content/5/6/eaaw4981, 2019.

Kleypas, J.: Modeled estimates of global reef habitat and carbonate production since the Last Glacial Maximum, Paleoceanography and Paleoclimatology, 12, 533–545, 1997.

Knox, F. and McElroy, M.: Changes in Atmospheric CO2: Influence of the Marine Biota at High Latitude, Journal of Geophysical Research, 89, 4269–4637, 1984.

Kohfeld, K. and Chase, Z.: Temporal evolution of mechanisms controlling ocean carbon uptake during the last glacial cycle, Earth and Planetary Science Letters, 472, 206–215, 2017.

Kohfeld, K. and Ridgewell, A.: Glacial-Interglacial Variability in Atmospheric CO2, Surface Ocean–Lower Atmosphere Processes, Geophysical Research Series, 187, 251–286, 2009.

Kohfeld, K., Quéré, C. L., Harrison, S., and Anderson, R.: Role of Marine Biology in Glacial-Interglacial CO2 Cycles, Science, 308, 74–78, 2005.

Kohler, P. and Fischer, H.: Simulating changes in the terrestrial biosphere during the last glacial/interglacial transition, Global and Planetary Change, 43, 33–55, 2004.

Köhler, P., Fischer, H., and Schmitt, J.: Atmospheric d13CO2 and its relation to pCO2 and deep ocean d13C during the late Pleistocene, Paleoceanography, 25, doi:10.1029/2008PA001 703, 2010.

Kohn, M.: Carbon isotope compositions of terrestrial C3 plants as indicators of (paleo)ecology and (paleo)climate, PNAS, 107, 19 691–19 695, 2010.

Kohn, M.: Carbon isotope discrimination in C3 land plants is independent of natural variations in pCO2, Geochemical Perspectives Letters, 2, 35–43, 2016.

Kurahashi-Nakamura, T., Paul, A., and Losch, M.: Dynamical reconstruction of the global ocean state during the Last Glacial Maximum, Paleoceanography, 32, 326–350, 2017.

Kwon, E., Primeau, F., and Sarmiento, J.: The impact of remineralization depth on the air–sea carbon balance, Nature Geoscience, 2, 630–635, 2009.

Lambert, F., Tagliabue, A., Shaffer, G., Lamy, F., Winckler, G., Farias, L., Gallardo, L., and Pol-Holz, D.: Dust fluxes and iron fertilization in Holocene and Last Glacial Maximum climates, Geophysical Research Letters, 42, 6014–6023, 2015.

Lindgren, A., Hugelius, G., and Kuhry, P.: Extensive loss of past permafrost carbon but a net accumulation into present-day soils, Letters to Nature, 560, 219–222, 2018.

Lisiecki, L. E. and Raymo, M. E.: A Pliocene-Pleistocene stack of 57 globally distributed benthic d18O records, Paleoceanography, 20, doi:10.1029/2004PA001 071, 2005.

Liu, C., Kohl, A., Liu, Z., Wang, F., and Stammer, D.: Deep-reaching thermocline mixing in the equatorial pacific cold tongue, Nature Communications, 7, 11 576, doi:10.1038/ncomms11 576, 2016.

Lourey, M. J. and Trull, W.: Seasonal nutrient depletion and carbon export in the Subantarctic and Polar Frontal Zones of the Southern Ocean south of Australia, Journal of Geophysical Research: Oceans, 106, 31 463–31 487, 2001.

Lueker, T. J., Dickson, A. G., and Keeling, C. D.: Ocean pCO2 calculated from dissolved inorganic carbon, alkalinity, and equations for K-1 and K-2: validation based on laboratory measurements of CO2 in gas and seawater at equilibrium, Marine Chemistry, 70, 105–119, 2000.

Maffezzoli, N., Vallelonga, P., Edwards, R., Saiz-Lopez, A., Turetta, C., Kjær, H. A., Barbante, C., Vinther, B., and Spolaor, A.: 120,000 year record of sea ice in the North Atlantic, Climate of the Past, 2018, 1–19, 2018.

Marchitto, T., Lehman, S., Ortiz, J., Flückiger, J., and van Geen, A.: Marine Radiocarbon Evidence for the Mechanism of Deglacial Atmospheric CO2 Rise, Science, 316, 1456–1459, 2007.

Martin, J.: Glacial-interglacial CO2 change: The Iron Hypothesis, Paleoceanography, 5, 1–13, 1990.

Martin, J. H., Knauer, G., Karl, D., and Broenkow, W.: VERTEX: carbon cycling in the northeast Pacific, Deep-Sea Research, 34, 267–285, 1987.

Martinez-Garcia, A., Sigman, D., H.Ren, Anderson, R., Straub, M., Hodell, D., Jaccard, S., Eglinton, T., and Haug, G.: Iron Fertilization of the Subantarctic Ocean During the Last Ice Age, Science, 343, 1347–1350, 2014.

Marzocchi, A. and Jansen, M. F.: Connecting Antarctic sea ice to deep-ocean circulation in modern and glacial climate simulations, Geophysical Research Letters, 44, 2017.

Matsumoto, K.: Biology-mediated temperature control on atmospheric pCO2 and ocean biogeochemistry, Journal of Geophysical Research, 34, L20 605, doi:10.1029/2007GL031 301, 2007.

Mauritz, M., Celis, G., Ebert, C., Hutchings, J., Ledman, J., Natali, S., Pegoraro, E., Salmon, V., Schädel, C., Taylor, M., , and Schuur, E.: Using stable carbon isotopes of seasonal ecosystem respiration to determine permafrost carbon loss, Journal of Geophysical Research: Biogeosciences, 124, 46–60, 2018.

Menviel, L. and Joos, F.: Toward explaining the Holocene carbon dioxide and carbon isotope records: Results from transient ocean carbon cycle-climate simulations, Paleoceanography, 27, PA1207, doi:10.1029/2011PA002 224, 2012.

Menviel, L., Joos, J., and Ritz, S.: Simulating atmospheric CO2, 13C and the marine carbon cycle during the Last Glacial-Interglacial cycle: possible role for a deepening of the mean remineralization depth and an increase in the oceanic nutrient inventory, Quaternary Science Reviews, 56, 46–68, 2012.

Menviel, L., Mouchet, A., Meissner, K. J., Joos, F., and England, M. H.: Impact of oceanic circulation changes on atmospheric d13CO2, Global Biogeochemical Cycles, 29, 1944–1961, 2015.

Menviel, L., Yu, J., Joos, F., Mouchet, A., Meissner, K. J., and England, M. H.: Poorly ventilated deep ocean at the Last Glacial Maximum inferred from carbon isotopes: A data-model comparison study, Paleoceanography, 31, 2–17, 2016.

Millero, F. J.: Influence of pressure on chemical processes in the sea. In Chemical Oceanography, 2nd edn, vol. 8, Academic Press, New York, 1983.

Morrison, A. and Hogg, A.: On the Relationship between Southern Ocean Overturning and ACC Transport, Journal of Physical Oceanography, 43, 140–148, 2013.

Morse, J. W. and Berner, R. A.: Dissolution kinetics of calcium carbonate in sea water. II: A kinetic origin for the lysocline, Am J Sci, 272, 1972.

Muglia, J., Skinner, L., and Schmittner, A.: Weak overturning circulation and high Southern Ocean nutrient utilization maximized glacial ocean carbon, Earth and Planetary Science Letters, 496, 47–56, 2018.

Muscheler, R., Beer, J., Wagner, G., Laj, C., Kissel, C., Raisbeck, G., Yioud, F., and Kubik, P.: Changes in the carbon cycle during the last deglaciation as indicated by the comparison of 10Be and 14C records, Earth and Planetary Science Letters, 219, 325–340, 2014.

Oliver, K., Hoogakker, B., Crowhurst, S., Henderson, G., Rickaby, R., Edwards, N., and Elderfield, H.: A synthesis of marine sediment core d13C data over the last 150 000 years, Climate of the Past, 6, 645–673, 2010.

O'Neill, C., A. Mc. Hogg, M.J. Ellwood, S. E., and Opdyke, B.: The [simple carbon project] model v1.0, Geosci. Model Dev., 12, 1541–1572, https://doi.org/10.5194/gmd–12–1541–2019, 2019.

Opdyke, B. and Walker, J.: Return of the coral reef hypothesis: Basin to shelf partitioning of CaCO3 and its effect on atmospheric CO2, Geology, 20, 733–736, 1992.

Otto, D., Rasse, D., Kaplan, J., Warnant, P., and Francois, L.: Biospheric carbon stocks reconstructed at the Last Glacial Maximum: comparison between general circulation models using prescribed and computed sea surface temperatures, Global and Planetary Change, 33, 117–138, 2002.

Peterson, C. D., Lisiecki, L. E., and Stern, J. V.: Deglacial whole-ocean d13C change estimated from 480 benthic foraminiferal records, Paleoceanography, 29, 549–563, 2014.

Piotrowski, A., Banakar, V., Scrivner, A., Elderfield, H., Galy, A., and Dennis, A.: Indian Ocean circulation and productivity during the last glacial cycle, Earth and Planetary Science Letters, 285, 179–189, 2009.

Prentice, I. C., Harrison, S., and Bartlein, P.: Global vegetation and terrestrial carbon cycle changes after the last ice age, New Phytologist, 189, 988–998, 2011.

Qin, B., Li, T., Xiong, Z., Algeo, T. J., and Chang, F.: Deepwater carbonate ion concentrations in the western tropical Pacific since 250 ka: Evidence for oceanic carbon storage and global climate influence, Paleoceanography, 32, 351–370, 2017.

Qin, B., Li, T., Xiong, Z., Algeo, T., and Jia, Q.: Deep-Water Carbonate Ion Concentrations in the Western Tropical Pacific Since the Mid-Pleistocene: A Major Perturbation During the Mid-Brunhes, Journal of Geophysical Research: Oceans, 123, https://doi.org/10.1029/2018JC014 084, 2018.

Reimer, P., Baillie, M., Bard, E., Bayliss, A., Beck, J., Blackwell, P., Ramsey, C. B., Buck, C., Burr, G., Edwards, R., Friedrich, M., Grootes, P., Guilderson, T., Hajdas, I., Heaton, T., Hogg, A., Hughen, K., Kaiser, K., Kromer, B., McCormac, F., Manning, S., Reimer, R., Richards, D., Southon, J., Talamo, S., Turney, C., van der Plicht, J., and Weyhenmeyer, C.: IntCal09 and Marine09 radiocarbon age calibration curves, 0-50,000 years cal BP., Radiocarbon, 51, 1111–50, 2009.

Ridgwell, A.: An end to the "rain ratio” reign?, Geochem. Geophys. Geosyst., 4, 1051, doi:10.1029/2003GC000 512, 2003.

Ridgwell, A., Watson, A., Maslin, M., and Kaplan, J.: Implications of coral reef buildup for the controls on atmospheric CO2 since the Last Glacial Maximum, Paleoceanography, 18, 1083, doi:10.1029/2003PA000 893, 2003.

Rohling, E., Grant, K., Bolshaw, M., Roberts, A., Siddall, M., Hemleben, C., and Kucera, M.: Antarctic temperature and global sea level closely coupled over the past five glacial cycles, Nature Geoscience, 2, 500–504, 2009.

Ronge, T., Tiedemann, R., Lamy, F., Kohler, P., Alloway, B., Pol-Holz, R. D., Pahnke, K., Southon, J., and Wacker, L.: Radiocarbon constraints on the extent and evolution of the South Pacific glacial carbon pool, Nature Communications, 7, 11 487, doi:10.1038/ncomms11 487, 2016.

Sarmiento, J. L. and Gruber, N.: Ocean biogeochemical dynamics, Princeton University Press, 2006.

Sarmiento, J. L. and Toggweiler, J. R.: A new model for the role of the oceans in determining atmospheric CO2, Nature, 308, 621–624, 1984.

Schmitt, J., Schneider, R., Elsig, J., Leuenberger, D., Lourantou, A., Chappellaz, J., Köhler, P., Joos, F., Stocker, T., Leuenberger, M., and Fischer, H.: Carbon Isotope Constraints on the Deglacial CO2 Rise from Ice Cores, Science, 336, 711–714, 2012.

Schneider, R., Schmitt, J., Kohler, P., Joos, F., and Fischer, H.: A reconstruction of atmospheric carbon dioxide and its stable carbon isotopic composition from the penultimate glacial maximum to the last glacial inception, Climate of the Past, 9, 2507–2523, 2013.

Schubert, B. and Jahren, A.: The effect of atmospheric CO2 concentration on carbon isotope fractionation in C3 land plants, Geochimica et Cosmochimica Acta, 96, 29–43, 2012.

Shaffer, G. and Lambert, F.: In and out of glacial extremes by way of dust-climate feedbacks, PNAS, 115, 2026–2031, 2018.

Siani, E., Michel, E., Pol-Holz, R. D., DeVries, T., Lamy, F., Carel, M., Isguder, G., Dewilde, F., and Lourantou, A.: Carbon isotope records reveal precise timing of enhanced Southern Ocean upwelling during the last deglaciation, Nature Communications, 4, 1–9, DOI: 10.1038/ncomms3758, 2013.

Siegel, D. A., Buesseler, K. O., Doney, S. C., Sailley, S. F., Behrenfeld, M. J., and Boyd, P. W.: Global assessment of ocean carbon export by combining satellite observations and foodweb models, Global Biogeochemical Cycles, 28, 181–196, 2014.

Sigman, D. and Boyle, E.: Glacial/interglacial variations in atmospheric carbon dioxide, Nature Reviews, 407, 859–869, 2000.

Sigman, D., Hain, M., and Haug, G.: The polar ocean and glacial cycles in atmospheric CO2 concentration, Nature Reviews, 466, 47–55, 2010.

Sikes, E., Samson, C., Guilderson, T., and Howard, W.: Old radiocarbon ages in the southwest Pacific Ocean during the last glacial period and deglaciation, Nature, 405, 555–559, 2000.

Sikes, E., Cook, M., and Guilderson, T.: Reduced deep ocean ventilation in the Southern Pacific Ocean during the last glaciation persisted into the deglaciation, Earth and Planetary Science Letters, 438, 130–138, 2016.

Skinner, L. and Shackleton, N. J.: Rapid transient changes in northeast Atlantic deep water ventilation age across Termination I, Paleoceanography, 19, PA2005, doi:10.1029/2003PA000 983, 2004.

Skinner, L., Waelbroeck, C., Scrivner, A., and Fallon, S.: Radiocarbon evidence for alternating northern and southern sources of ventilation of the deep Atlantic carbon pool during the last deglaciation, PNAS, 111, 2014.

Skinner, L., McCave, I., Carter, L., Fallon, S., Scrivner, A., and Primeau, F.: Reduced ventilation and enhanced magnitude of the deep Pacific carbon pool during the last glacial period, Earth and Planetary Science Letters, 411, 45–52, 2015.

Skinner, L., Primeau, F., Freeman, E., de la Fuente, M., Goodwin, P. A., Gottschalk, J., Huang, E., McCave, I. N., Noble, T. L., and Scrivner, A. E.: Radiocarbon constraints on the glacial ocean circulation and its impact on atmospheric CO2, Nature Communications, 8, 16 010, doi: 10.1038/ncomms16 010, 2017.

Skinner, L. C., Fallon, S., Waelbroeck, C., Michel, E., and Barker, S.: Ventilation of the Deep Southern Ocean and Deglacial CO2 Rise, Science, 328, 1147–1151, 2010.

Stephens, B. and Keeling, R.: The infuence of Antarctic sea ice on glacial-interglacial CO2 variations, Nature, 404, 171–174, 2000.

Stott, L., Southon, J., Timmermann, A., and Koutavas, A.: Radiocarbon age anomaly at intermediate water depth in the Pacific Ocean during the last deglaciation, Paleoceanography, 24, 2009.

Strutz, T.: Data Fitting and Uncertainty. A practical introduction to weighted least squares and beyond., vol. 2 of *Wiesbaden*, Springer Vieweg, 2016.

Takahashi, T., Sutherland, S., Feely, R., and Cosca, C.: Decadal variation of the surface water PCO2 in the western and central equatorial Pacific, Science, 302, 852–856, 2003.

Talley, L.: Closure of the global overturning circulation through the Indian, Pacific, and Southern Oceans: Schematics and transports, Oceanography, 78, 257–303, 2013.

Tarnocai, C., Canadell, J., Schuur, E., Kuhry, P., Mazhitova, G., and Zimov, S.: Soil organic carbon pools in the northern circumpolar permafrost region, Global Biogeochemical Cycles, 23, GB2023, doi:10.1029/2008GB003 327, 2009.

Toggweiler, J. and Sarmiento, J.: Glacial to interglacial changes in atmospheric carbon dioxide: The critical role of ocean surface water in high latitudes, in The Carbon Cycle and Atmospheric CO2: Natural Variations Archean to Present, Geophysical Monograph Series, American Geophysical Union, 32, 163–184, 1985.

Toggweiler, J. R.: Variation of atmospheric CO2 by ventilation of the ocean's deepest water, Paleoceanography, 14, 571–588, 1999.

Toggweiler, J. R.: Origin of the 100,000-year time scale in Antarctic temperatures and atmospheric CO2, Paleoceanography, 23, PA2211, doi:10.1029/2006PA001 405, 2008.

Treat, C., Kleinen, T., Broothaerts, N., Dalton, A., Dommain, R., Douglas, T., Drexler, J., Finkelstein, S., Grosse, G., Hope, G., Hutchings, J., Jones, M., Kuhry, P., Lacourse, T., Lähteenoja, O., Loisel, J., Notebaert, B., Payne, R., Peteet, D., Sannel, A., Stelling, J., Strauss, J., Swindles, G., Talbot, J., Tarnocai, C., Verstraeten, G., C.J. Williams, Z. X., Yu, Z., Väliranta, M., Hättestrand, M., Alexanderson, H., and Brovkin, V.: Widespread global peatland establishment and persistence over the last 130,000 y, PNAS, 116, 4822–4827, 2019.

van der Sleen, P. et al.: No growth stimulation of tropical trees by 150 years of CO2 fertilization but water-use efficiency increased, Nature Geoscience, 8, 2015.

Vecsei, A. and Berger, W.: Increase of atmospheric CO2 during deglaciation: Constraints on the coral reef hypothesis from patterns of deposition, Global Biogeochemical Cycles, 18, GB1035, doi:10.1029/2003GB002 147, 2004.

Watson, A., Bakker, D. C. E., Ridgwell, A. J., Boyd, P. W., and Law, C.: Effect of iron supply on Southern Ocean CO2 uptake and implications for glacial atmospheric CO2, Nature, 407, 730–733, 2000.

Weeding, B. and Trull, W.: Hourly oxygen and total gas tension measurements at the Southern Ocean time series site reveal winter ventilation and spring net community production, Journal of Geophysical Research: Oceans, 119, 348–358, 2004.

Wolff, E., Barbante, C., Becagli, S., Bigler, M., Boutron, C., Castellano, E., de Angelis, M., Federer, U., Fischer, H., Fundel, F., Hansson, M., Hutterli, M., Jonsell, U., Karlin, T., Kaufmann, P., Lambert, F., Littot, G., Mulvaney, R., Roöthlisberger, R., Ruth, U., Severi, M., Siggaard-Andersen, M., Sime, L., Steffensen, J., Stocker, T., Traversi, R., Twarloh, B., Udisti, R., Wagenbach, D., and Wegner, A.: Changes in environment over the last 800,000 years from chemical analysis of the EPICA Dome C ice core, Quaternary Science Reviews, 29, 285–95, 2010.

Yamamoto, A., Abe-Ouchi, A., Ohgaito, R., Ito, A., and Oka, A.: Glacial CO2 decrease and deep-water deoxygenation by iron fertilization from glaciogenic dust, Climate of the Past, 15, 981–996, 2019.

Yu, J., Broecker, W., Elderfield, H., Jin, Z., McManus, J., and Zhang, F.: Loss of Carbon from the Deep Sea Since the Last Glacial Maximum, Science, 330, 1084–1087, 2010.

Yu, J., Anderson, R., Jin, Z., Rae, J., Opdyke, B., and Eggins, S.: Responses of the deep ocean carbonate system to carbon reorganization during the Last Glacial-interglacial cycle, Quaternary Science Reviews, 76, 39–52, 2013.

Yu, J., Anderson, R., Z.Jin, Menviel, L., Zhang, F., Ryerson, F., and Rohling, E.: Deep South Atlantic carbonate chemistry and increased interocean deep water exchange during last deglaciation, Quaternary Science Reviews, 90, 80–89, 2014a.

Yu, J., Anderson, R. F., and Rohling, E. J.: Deep ocean carbonate chemistry and glacial-interglacial atmospheric CO2 changes, Oceanography, 27, 16–25, 2014b.

Yu, J., Menviel, L., Jin, Z. D., Thornalley, D., Barker, S., Marino, G., Rohling, E. J., Cai, Y., Zhang, F., Wang, X., Dai, Y., Chen, P., and Broecker, W. S.: Sequestration of carbon in the deep Atlantic during the last glaciation, Nature Geoscience, 9, 319–325, 2016.

Yu, J., Menviel, L., Jin, Z., Thornalley, D., Foster, G., Rohling, E., McCave, I., McManus, J., Dai, Y., Ren, H., He, F., Zhang, F., Chen, P., and Roberts, A.: More efficient North Atlantic carbon pump during the Last Glacial Maximum, Nature Communications, 10, https://doi.org/10.1038/s41 467–019–10 028–z, 2019.

Zhao, N., Marchal, O., Keigwin, L., Amrhein, D., and Gebbie, G.: A Synthesis of Deglacial Deep-Sea Radiocarbon Records and Their (In)Consistency With Modern Ocean Ventilation, Paleoceanography and Paleoclimatology, 33, 128–151, 2017.